Atmos. Chem. Phys. Discuss., 13, 30349–30405, 2013
www.atmos-chem-phys-discuss.net/13/30349/2013/
doi:10.5194/acpd-13-30349-2013

Atmospheric Chemistry and Physics Discussions
Open Access

Surface sensible and latent heat fluxes over the Tibetan Plateau from ground measurements, reanalysis, and satellite data

Q. Shi[1] and S. Liang[1,2,3]

[1]Department of Geographical Sciences, University of Maryland, College Park, Maryland, USA
[2]State Key Laboratory of Remote Sensing Science, Jointly Sponsored by Beijing Normal University and the Institute of Remote Sensing Applications of Chinese Academy of Sciences, Beijing, China
[3]College of Global Change and Earth System Science, Beijing Normal University, Beijing, China

Received: 3 September 2013 – Accepted: 2 November 2013 – Published: 21 November 2013

Correspondence to: Q. Shi (qshi@umd.edu)

Published by Copernicus Publications on behalf of the European Geosciences Union.

Surface sensible and latent heat fluxes over the Tibetan Plateau

Q. Shi and S. Liang

Abstract

Estimations from meteorological stations indicate that the surface sensible heat flux over the Tibetan Plateau (TP) has been decreasing continuously since 1980s, and modeling studies suggest that such changes are likely linked to the weakening of the East Asian Monsoon through exciting Rossby wave trains. However, the spatial and temporal variations in the surface sensible and latent heat fluxes over the entire TP remain unknown. This study aims to characterize the monthly surface sensible and latent heat fluxes at 0.5° over the TP from 1984 to 2007 by synthesizing multiple data sources including ground measurements, reanalysis products, and remote sensing products. The root mean square errors (RMSEs) from cross-validation are 11.1 $\mathrm{W\,m^{-2}}$ and 17.8 $\mathrm{W\,m^{-2}}$ for the monthly fused sensible and latent heat fluxes, respectively. The fused sensible and latent heat flux anomalies are consistent with those estimated from meteorological stations, and the uncertainties of the fused data are also discussed. The annual sensible heat flux over the TP is shown to be decreasing by $-1.1\,\mathrm{W\,m^{-2}\,deacade^{-1}}$ with dominant decreasing in summer ($-3.9\,\mathrm{W\,m^{-2}\,deacade^{-1}}$), while the latent heat flux shows a decrease (increase) in spring (autumn) but at a magnitude less than that of the sensible heat flux. Such decreased tendency of the fused sensible and latent heat flux over the TP is consistent to the weakened East Asian Monsoon as well as the solar dimming. The associations among sensible and latent heat fluxes and the related surface anomalies such as mean temperature, temperature range, snow cover, and Normalized Difference Vegetation Index (NDVI) in addition to atmospheric anomalies such as cloud cover and water vapor show seasonal dependence, suggest that the land–biosphere–atmosphere interactions over the TP could display nonuniform feedbacks to the climate changes. It would be interesting to disentangle the drivers and responses of the surface sensible and latent heat flux anomalies over the TP in future research from evidences of modeling results.

1 Introduction

The land surface energy balance (SEB) is a critical physical characteristic of land surface processes. It states the ability of the land surface to partition the net radiation (NR) into latent heat flux (LE), sensible heat flux (H), and ground heat flux (G) (Eq. 1), which governs the hydrological, biogeochemical, and ecological processes at the Earth's surface (Liang et al., 2010):

$$\mathrm{NR} = \mathrm{LE} + H + G \quad (1)$$

In contrast to the global land SEB that has been accessed by using surface observations, remote sensing, and reanalysis datasets, less attention has been paid to analyze the spatiotemporal characteristics of the land SEB at the regional scale due to the limit representative of ground observation and the lack of comprehensive validation (Kiehl and Trenberth, 1997; Trenberth et al., 2009; Jung et al., 2011; Stephens et al., 2012; Stevens and Schwartz, 2012; Wild, 2012). Although limited long-term ground observations measure the SEB, the decadal changes of evapotranspiration have been quantified empirically by using ground measurements and remote sensing observations (Wang and Liang, 2008; Jung et al., 2010; Yao et al., 2012). However, it is important to conduct comprehensive validation and intercomparison before applying global datasets at the regional scale, because the confidence of such datasets relies largely on the characteristics of the inputs such as homogeneity of satellite products and distribution of stations (Mueller et al., 2013).

The SEB over the Tibetan Plateau (TP) is of great research interest because of its physical links to the East Asian Monsoon, which sustains approximately 25 % of the world's population (Wang and Liang, 2008; Immerzeel et al., 2010). At the geological scale, numerical experiments and geologic observations have supported the theory such that the formation of the Asian monsoon is related to the uplift of the TP (Kutzbach et al., 1993; An et al., 2001). In addition to the mechanical forcing of the TP through partitioning of the jet stream (Manabe and Terpstra, 1974), physical processes by which the thermal forcing of the TP is linked to the onset and strength of the

ACPD
13, 30349–30405, 2013

Asian monsoon have been inferred from the shift of the jet stream, the formation of the south Asian High, the diurnal variation of meteorological observations of the TP, and numerical experiments (Ye and Gao, 1979; Yanai and Li, 1994; Ye and Wu, 1998; Wu et al., 2012a). The concept of "sensible-heat driven air-pump" over the TP has been proposed in research of the elevated heating effect over the TP by using the global circulation model (GCM) (Wu et al., 2007). This concept suggests that the surface heating (cooling) in summer (winter) causes air column to converge (diverge) and to ascend (descend), regulating both local and Northern Hemisphere circulation. Furthermore, such processes create the south Asian High in the upper atmosphere in summer and the increasingly high pressure over continental areas in winter, likely contributing to the pattern of droughts in the north and floods in the south in China in addition to the country's cold continental climate, respectively (Duan et al., 2013).

The SEB over the TP is essential for the study of land–biosphere–atmosphere interactions, analysis of the changes in terrestrial ecosystems and hydrological systems, and assessment of the impacts of and feedbacks to the climate changes. Previous research has investigated the diurnal, seasonal and annual variation of the SEB of stations over various land cover types in the TP, including grassland (Ma et al., 2003; Tanaka et al., 2003; Liu et al., 2009; Bian et al., 2012), meadow (Gu et al., 2005; Yao et al., 2008, 2011), and glacial and alpine areas (Zou et al., 2009; Yang et al., 2011d; Chen et al., 2012; Zhang et al., 2013). Advanced methods have been developed to retrieve SEB from improved parameterization of routine meteorological observations (Yang et al., 2002, 2003, 2008; Chen et al., 2010, 2013b; Guo et al., 2011b; Lee et al., 2012) satellite observations (Ma et al., 2006, 2009, 2011a, 2012; Jiménez et al., 2009; Zhang et al., 2010), and the integration of both data sources (Wang and Liang, 2008; Jung et al., 2009; Yao et al., 2012). The uncertainties of those approaches in characterizing the SEB over the TP, however, remain large, resulting in misrepresentation and inconsistency of the inferred decadal changes of the sensible heat flux from reanalysis or the conventional bulk aerodynamic method (Yang et al., 2011b; Zhu et al., 2012). Specifically, observation-based results are inadequate for determining the regional pat-

ACPD
13, 30349–30405, 2013

tern of the SEB over the entire TP due to the unbalanced distribution of meteorological stations and the sparse temporal coverage of the remote sensing products under the requirement of clear-sky conditions (Ma et al., 2006, 2011b), whereas the reliability of modeling results is largely limited not only by the propagation of input error through the model retrieval (Wang and Dickinson, 2012), but also by the uncertainty of parameterization under complex terrain and highly heterogeneous areas (Chen et al., 2013a). Instead, GCMs have been applied extensively to access the effects of warming (Wang et al., 2008, 2011), snow forcing (Qian et al., 2011; Turner and Slingo, 2011), and weakened sensible heat flux (Liu et al., 2012; Wu et al., 2012a; Duan et al., 2013) over the TP on the precipitation changes in East Asia. Nevertheless, gaps remain in quantification of the decadal changes of the SEB over the TP at the regional scale in comparison with changes derived from ground observations and in assessment of the relationship between the changes of the SEB and the observed surface and atmospheric conditions.

The objective of this study is to analyze the spatiotemporal characteristics of the surface sensible and latent heat fluxes over the TP by integrating ground observations, remote sensing, and reanalysis datasets over the recent two decades. The following sections introduce various data sources and methodologies including preprocessing, data fusion, and spatiotemporal characterization; describe the validation results; investigate the spatiotemporal patterns and decadal changes; discuss uncertainties including energy closure, sensitivity to scale and model choices, and intercomparison to other datasets; and conclude with major findings and implications derived from the results.

2 Datasets

The TP includes areas with elevations higher than 3000 m within approximately 30° longitude (75–105° E) and 14° latitude (26–40° N) (Fig. 1). To integrate observational and modeling results of the SEB over the TP, the following three sources data were

ACPD
13, 30349–30405, 2013

included: (1) ground measurement data from AsiaFlux, ChinaFLUX, GAME/Tibet, and CAMP/Tibet; (2) state-of-the-art reanalysis products from the Climate Forecast System Reanalysis (CFSR), the Modern-Era Retrospective analysis for Research and Applications (MERRA), the ERA-Interim reanalysis, and the Japanese 25 yr Reanalysis (JRA-25); and (3) a remote sensing-based product from a global evapotranspiration model developed by Zhang et al. (2010), hereafter referred to as Zhang10 (Table 1).

2.1 Ground-measured datasets

Surface energy fluxes based on ground measurement were extracted from three sources including the Coordinated Energy and Water Cycle Observation Project (CEOP) (Koike, 2004), the Asian Automatic Weather Station Network (ANN) (Sugita et al., 2005), and FLUXNET (Baldocchi et al., 2001). Over an 11 yr period in 1997–2007, ground SEB measurements from 13 stations were selected from the AsiaFlux sites (Kim et al., 2009), the ChinaFLUX sites (Yu et al., 2006), the Global Energy and Water Cycle Experiment (GEWEX) Asian Monsoon Experiment on the TP (GAME/Tibet; http://monsoon.t.u-tokyo.ac.jp/tibet), and the CEOP Asia–Australia Monsoon Project on the TP (CAMP/Tibet; http://data.eol.ucar.edu/codiac/dss/id=76.127). To ensure independency of the ground observations, those stations were checked for exclusion in the development of remote sensing and reanalysis products. The critical information used in station selection for extracting high-quality SEB measurements includes location, measured variables, measured height, instruments, data period, and number of days (Table 2). The ground heat flux is recorded by a soil heat flux plate at a height below the surface ranging from 0.01 m to 0.1 m deep with expected accuracy by ±5 % of reading for Campbell HFT-3 and EKO MF-81, and $-15 \sim +5$ % of the 12 h total for Hukseflux HFP01. The eddy-covariance method measures sensible and latent heat fluxes from high-frequency flux covariance (by 10 Hz) of the wind vector from a three-dimensional sonic anemometer (Campbell CSAT-3, GILL SAT-R3A, and Kaijo DA-600) and the humidity fluctuation from an open-path infrared gas analyzer (LI-COR LI-7500 and Kaijo AH-300), a krypton hygrometer (Campbell KH20), or a thermohygrometer (Vaisala 50Y Bandpass TRH). Based on the manufactory specifications, the estimated accuracy of GILL SAT-R3A is $< 1\,\%$ root–mean–square (RMS) of the reading; LI-COR LI-7500, $\pm 2\,\%$ of the reading; Campbell KH20, $\pm 5\,\%$ of the reading; and Campbell CSAT-3, $\pm 6\,\%$ of the horizontal as gain error and $\pm 8.0\,\mathrm{cm\,s^{-1}}$ ($\pm 4.0\,\mathrm{cm\,s^{-1}}$) of horizontal (vertical) offset error. The typical estimated error of the eddy-covariance measurements is 5–20 % including 20–50 $\mathrm{W\,m^{-2}}$ and 10–30 $\mathrm{W\,m^{-2}}$ for latent heat and sensible heat fluxes, respectively (Foken, 2008).

As regional branches of FLUXNET, AsiaFlux and ChinaFLUX measure carbon cycle, hydrological cycle, and energy exchange to study the interaction between the terrestrial ecosystem and the atmosphere. The AsiaFlux site, an alpine meadow grassland in Haibei (HBM), China, offers 15 min averaged SEB measurements, which removes unreliable data by using absolute threshold quality control (Vickers and Mahrt, 1997). The longest measurements of the SEB over the TP are acquired from two ChinaFLUX sites where SEB is averaged at 30 min intervals after applying the correction for the density effect to latent heat flux from 2003 to 2007 at the Damxung site (DX) and from November 2002 to 2007 at the Haibei Shrubland site (HBS) (Webb et al., 1980).

GAME/Tibet and CAMP/Tibet are organized by international monsoon experiments. 30 min SEB averages were extracted from GAME/Tibet during the intensive observation period (IOP) in 1998, which included portable automated mesonets (PAM) at MS3478, planetary boundary layer (PBL) tower measurements of radiation fluxes and turbulent flux measurements at Amdo and BJ stations, respectively. CAMP/Tibet radiation and flux datasets were collected during the Enhanced Observing Period 3 (EOP-3) and Enhanced Observing Period 4 (EOP-4) of CEOP, covering the period from October 2002 to December 2004. Six stations including Amdo, ANNI, D105, MS3478, BJ, and Gaize measured soil heat flux from 0.2 Hz samples and averages at 10 min intervals. Comprehensive measurements have been taken at the BJ site, including 3 m latent and sensible heat fluxes averaged over 30 min intervals. Heat fluxes from CAMP/Tibet were visually examined for low and high extreme or constant values by using the CAMP Quality Control Web Interface; data with quality flags of good or in-

ACPD
13, 30349–30405, 2013

terpolated were used in this study. Because most sites share the same locations with GAME/Tibet but use different instruments, observations from multiple datasets of the same sites were combined before analysis.

Two datasets based on meteorological station data over the TP reported by (Yang et al., 2009) and (Yang et al., 2011a), hereafter referred to as Yang09 and Yang11, respectively, were chosen for comparison purposes. Yang09 estimates the daily sensible heat flux of 85 stations over the TP by using a micro-meteorological method, which is a physical scheme similar to the eddy-covariance method but includes statistical downscaled wind speed and ground-air temperature from the China Meteorological Administration (CMA) stations. The advantage of the Yang09 scheme over conventional methods is that it produces a realistic estimation of the sensible heat flux by accounting for the diurnal variation of the heat transfer process (Yang et al., 2011b). Based on the 250 m Normalized Difference Vegetation Index (NDVI) from the global Moderate Resolution Imaging Spectroradiometer (MODIS) vegetation indices product (MOD13Q1), data of 59 stations with elevations > 3000 m under the NDVI < 0.2 and snow-free conditions were selected by considering the quality flag of MOD13Q1 because of the suitability of the Yang09 scheme for bare soil or spares vegetation land cover. Yang11 provides the simulation results of the SEB of the CMA stations over the TP by using the SiB2 adjusted land surface model (Sellers et al., 1996) according to the TP surface characteristics reported from previous experiments (Yang et al., 2008). In recent studies, the climatology and trend of sensible heat flux over the TP extracted from Yang11 have been compared to that from reanalysis datasets, suggesting a general weakened trend of the sensible heat source over the TP in recent decades, with large uncertainties among different datasets (Liu et al., 2012; Zhu et al., 2012).

2.2 Remote sensing datasets

Remote sensing-based estimations of evapotranspiration have been developed to access decadal changes of evapotranspiration over the pan-Arctic basin and Alaska (Zhang et al., 2009), which were then applied to the global land surface (Zhang

ACPD
13, 30349–30405, 2013

et al., 2010). Zhang10 estimates evapotranspiration over vegetated areas by a modified Penman–Monteith approach with a biome-specific canopy conductance model parameterized from 34 FLUXNET sites. The major inputs are NDVI from the Advanced Very High Resolution Radiometer (AVHRR) provided by NASA Global Inventory Modeling and Mapping Studies (GIMMS) (Tucker et al., 2005), air temperature and water vapor pressure from the National Center of Environmental Prediction (NCEP)/National Center for Atmospheric Research (NCAR) (NCEP/NCAR) reanalysis version 1 (NRA-1) (Kalnay et al., 1996), and shortwave radiation from GEWEX Surface Radiation Budget (GEWEX SRB 3.0) (Pinker and Ewing, 1985; Pinker and Laszlo, 1992). The independent validation over 48 FLUXNET sites including HBM satisfied accuracy at $R^2 = 0.80$–0.84. A recent evaluation of Zhang10 suggests that it outperforms other reanalysis and remote sensing datasets over the upper Yellow River and Yangtze River basins in the TP (Xue et al., 2013).

2.3 Reanalysis datasets

The NCEP CFSR is the first global reanalysis product to apply a coupled land–atmosphere–ocean–sea ice system (Saha et al., 2010). The land surface analysis is produced from the Noah land surface model, which is forced by the output from the atmospheric assimilation in addition to observed precipitation and snow depth (Ek et al., 2003). This model outperforms the previous NCEP reanalysis datasets with higher spatial resolution (T382, approximately 0.31°) and improved land surface energy and water closures at the monthly scale (Meng et al., 2012). MERRA, a recent reanalysis dataset supported by NASA's Global Modeling and Assimilation Office (GMAO) covering temporal period since 1979, incorporates a catchment hydrological model (Koster and Suarez, 1996; Koster et al., 2000) and a multi-layer snow model (Stieglitz et al., 2001) that are coupled to the GOES-5 atmospheric GCM. Global assessments suggest an improvement in the hydrological cycles with MERRA (Rienecker et al., 2011). ERA-Interim is the first reanalysis product to apply the four-dimensional variational data assimilation scheme (4D-Var) provided by the European Centre for Medium-Range

ACPD
13, 30349–30405, 2013

Surface sensible and latent heat fluxes over the Tibetan Plateau

Q. Shi and S. Liang

Weather Forecasts (ECMWF) (Dee et al., 2011), which assimilates 2 m air temperature and humidity to correct soil moisture and temperature analyses (Douville et al., 2000). The Tiled ECMWF Scheme for Surface Exchanges over Land (TESSEL) (Viterbo and Beljaars, 1995; Viterbo and Betts, 1999) and the snow scheme (Douville et al., 1995) are used in the ERA-Interim for modeling land surface processes. JRA-25 aims to provide high-quality data for the Asian region by applying the Japan Meteorological Agency (JMA) numerical assimilation and forecast system (Onogi et al., 2007). A simple biosphere scheme is used in JRA-25 with observed snow data (Sellers et al., 1986; Sato et al., 1989). A recent comparison has revealed consistency in the interannual variability and a weakened tendency of surface wind speed and sensible heat flux over the TP among JRA-25, Yang11, and NRA-1, whereas large interannual variation and inconsistency have been identified for CFSR (Zhu et al., 2012).

3 Methodology

Monthly mean SEB components over the TP were extracted from ground measurements, remote sensing, and reanalysis datasets. Original ground-measured values of surface latent heat flux, sensible heat flux, and ground heat flux were first converted to Coordinated Universal Time (UTC) and were then integrated to daily hourly mean by using quality control flags to exclude poor-quality and missing data and by corresponding thresholds of −200–400 $W m^{-2}$, −200–500 $W m^{-2}$, and −200–300 $W m^{-2}$. The surface energy balance was closed by using the observed Bowen ratio on the daily scale (Twine et al., 2000). Daily averages of the SEB components were also extracted from the original reanalysis datasets, followed by interpolation to 0.5° resolution by using the nearest grid data from MERRA, Interim, and JRA-25 or the mean grids value covered by the newly projected grid from CFSR. The monthly mean value was calculated from the daily mean covering more than 15 days in a month. Similar interpolation was applied to Zhang10 monthly data, which was converted to latent heat flux by multiplying the latent heat of vaporization, λ (2.451 $MJ kg^{-1}$). The sensible heat flux of Zhang10

ACPD
13, 30349–30405, 2013

is estimated from the difference between the net radiation from GEWEX SRB 3.0 and the latent heat flux from Zhang10, assuming the ground heat flux is relatively small and negligible (Jiménez et al., 2011).

The multiple linear regression (MLR) method was used to fuse remote sensing and reanalysis datasets with ground observations. The data fusion approach synthesizes multiple sources of data to improve accuracy, confidence, and consistency of the results, and the MLR has the advantage of being simple and easily interpreted. The MLR model, using p original datasets (X_i) and the truth (Y) from the ground-measured data, is expressed as

$$Y = \beta_0 + \sum_{i=1}^{p} \beta_i \times X_i + \varepsilon, \varepsilon \sim N(0, \sigma^2), \quad p > 1 \tag{2}$$

where β_i (β_0) is the coefficient (intercept) and ε is the residual assumed to be normally distributed ($N(0,\sigma^2)$). The intercept and coefficients are determined to minimize the sum of the square residuals. This study applied MLR to latent and ground heat fluxes. A monthly fused surface radiation budget at 0.5° over the TP has been developed, which addresses the relative low accuracy of surface radiation budget from individual remote sensing or reanalysis product and the sparse ground radiation measurements by integrating multiple datasets (Shi and Liang, 2013a). The sensible heat flux was estimated from the energy balance (Eq. 1) by subtracting the latent heat and ground heat fluxes (this study) from the previously developed net radiation (Shi and Liang, 2013a). The reason of this approach is to constrain uncertainty (see Sect. 5.2.2 for details). To ensure energy closure, only the stations with all SEB component measurements were used in the data fusion of the latent heat flux. Three types of statistics including RMS error (RMSE), mean bias error (MBE), and coefficient of determination (R^2) were used to quantify the accuracy of each input product. The RMSE from the leave-one-out cross-validation, hereafter referred to as RMSE_CV, was used to validate the fused SEB components.

Comparisons were performed among monthly average values over all available stations and seasonal and annual anomalies over CMA stations from 1984 to 2006. The

ACPD
13, 30349–30405, 2013

spatial pattern of the seasonal and annual average and the standard deviation (STD) of the latent and sensible heat fluxes over the TP were analyzed, and the decadal changes of latent and sensible heat fluxes during 1984 to 2007 were detected by using the linear regression method and Student's *t* test for significance for an annual period and for four seasons including spring (March-April-May, MAM), summer (June-July-August, JJA), autumn (September-October-November, SON), and winter (December-January-February, DJF). The interannual variability from the average latent and sensible heat flux anomalies over the TP was compared to the selected indicators of atmospheric and surface conditions and the fused surface radiation budget anomalies (Shi and Liang, 2013b), the relationships of which were quantified by using the Pearson correlation coefficient. The selected variables included cloud cover and temperature (monthly mean of daily mean temperature and temperature range) from the Climate Research Unit (CRU) TS3.1 (Mitchell and Jones, 2005), Rutgers snow cover data (Robinson et al., 1993), the GIMMS AVHRR NDVI (Tucker et al., 2005), and MERRA water vapor.

4 Results

4.1 Validation results

The validation results of CFSR, MERRA, ERA-Interim, JRA-25, and Zhang10 are shown in Table 3. The latent heat flux from all five products had significantly higher R^2 (> 0.8) and smaller RMSEs of the latent heat flux than those of sensible heat flux. The absolute value of MBE and RMSE of the ground heat flux were smaller than those of latent and sensible heat fluxes. CFSR underestimated latent and sensible heat fluxes by $-13.1\,\mathrm{W\,m^{-2}}$ and $-4.9\,\mathrm{W\,m^{-2}}$, respectively, and overestimated G by $6.6\,\mathrm{W\,m^{-2}}$. The RMSE of the latent heat flux from CFSR was the largest among all reanalysis datasets. MERRA and JRA-25 overestimated the latent heat flux with RMSE by $15\,\mathrm{W\,m^{-2}}$. MERRA (JRA-25) exhibited the lowest R^2 (largest RMSE) in the sensible

ACPD
13, 30349–30405, 2013

heat flux of all reanalysis datasets. Latent and sensible heat fluxes from the ERA-Interim at 11.5 $W m^{-2}$ and 20.5 $W m^{-2}$, respectively were the most accurate among other four products with the lowest RMSE. Zhang10 had a high R^2 by 0.89 but showed underestimation of −12.0 $W m^{-2}$ of the latent heat flux.

The coefficients and intercepts used to calculate the ground heat flux and the fused latent heat flux with and without Zhang10 were derived by using the MLR method (Table 4). Similar to the significant large interannual variation of the sensible heat flux from CFSR over the TP (Zhu et al., 2012), the latent heat flux from CFSR was excluded in data fusion because it exhibits significant large interannual variation and large RMSE over the TP. Zhang10 and JRA-25 had the largest coefficient in the latent heat and ground heat fluxes, respectively. Under the condition such that Zhang10 was missing, ERA-Interim and MERRA mainly dominated the fused latent heat flux. The fused datasets exhibited the lowest RMSE_CV over that by using individual datasets for the latent heat, ground heat, and sensible heat fluxes by 11.1 $W m^{-2}$, 2.6 $W m^{-2}$, and 17.8 $W m^{-2}$, respectively (Table 5). The cross-validation results support that no individual reanalysis dataset is supreme in all SEB components and that a synthesized approach that uses MLR could be a feasible way for improving the accuracy. After using data from all available stations, the plots in Fig. 2 between the ground measurement and the fused results indicate that the latent heat flux was closer to the 1 : 1 line than the other two components. RMSEs of the fused latent heat flux, sensible heat flux, and ground heat flux were 7.9 $W m^{-2}$, 12.5 $W m^{-2}$, and 2.4 $W m^{-2}$, respectively, which significantly improved the R^2 of the sensible heat flux by 0.61. The accuracy of the data fusion method is sensitive to the training data, which explains the decreased value of RMSE from RMSE_CV. An independent validation of the sensible heat flux by using Yang09 also indicated that the fused H had the lowest RMSE, by 16.7 $W m^{-2}$, than that by using individual reanalysis datasets, which ranged from 22.1 $W m^{-2}$ to 26.0 $W m^{-2}$.

A comparison was also performed with other global datasets that were available during the validation period (Table 5). The selected datasets include MERRALAND as the supplementary product, which uses the revised MERRA land system forced with

ACPD
13, 30349–30405, 2013

observed precipitation (Reichle et al., 2011); empirically estimated latent and sensible heat fluxes from FLUXNET stations and remote sensing observations that use model tree ensembles (MTE-LE-H) (Jung et al., 2009, 2010, 2011); a global land evapotranspiration dataset reported by a Princeton University study on the basis of a revised Penman–Monteith model that used radiation-forcing data from GEWEX SRB 3.0 (PU-ET) (Mu et al., 2007; Vinukollu et al., 2011); and four SEB components from the Global Land Data Assimilation Systems (Rodell et al., 2004), which uses three off-line models including the Common Land Model version 2.0 (GLDAS-1-CLM) (Oleson et al., 2004), the Mosaic Model (Koster and Suarez, 1996) (GLDAS-1-MOS), and the National Centers for Environmental Prediction/Oregon State University/Air Force/Hydrologic Research Lab Model version 2.7 (Chen et al., 1997; Ek et al., 2003) (GLDAS-1-NOAH, GLDAS-2-NOAH). Overall, the fused latent and sensible heat fluxes outperformed the datasets in terms of lower RMSE_CVs. Although MPI-ET and PU-ET showed consistent positive (negative) trends before (after) 1998 over global land, large uncertainties from input-forcing limit the use to indicate the actual trend and long-term variability of evapotranspiration (Wang and Dickinson, 2012). Therefore, the validation and intercomparison of the SEB over the area in which sparse ground observations are used to constrain the data-driven models (i.e., MTE-LE-H) or the parameterization of the land surface model less turned to adjust to the local conditions must be implemented before using global datasets for regional studies.

4.2 Seasonal and interannual variability

The comparison of the monthly cycle averaged over all available stations showed more consistent seasonal cycles of latent heat and the ground heat fluxes than that of the sensible heat flux from reanalysis and remote sensing datasets (Fig. 3). The ground heat flux from the reanalysis datasets had a positive (negative) bias in MAM and JJA (DJF). MERRA, JRA-25, and Zhang10 overestimated the latent heat flux in DJF, which was significantly underestimated by CFSR and Zhang10 by $> 20\,\mathrm{W\,m^{-2}}$ from May to September. Although the number of stations is small, the consistent seasonal cycles

ACPD
13, 30349–30405, 2013

from remote sensing and reanalysis datasets enhance the confidence for the climatology and monthly accuracy of latent heat flux over the central and eastern TP. MERRA exhibited large fluctuation for sensible heat flux in JJA and SON; CFSR and JRA-25 showed a similar pattern but with less value and variability; and Zhang10 (ERA-Interim) had a smooth variation with a peak in May (March). A comparison with the monthly cycles of CMA stations from Yang09 over bare land and sparsely vegetated areas indicates that the fused sensible heat flux was closer to that from Yang09, particularly from January to August. The differences in seasonal variability of the sensible heat flux in SON and in early DJF (when fused sensible heat flux is closer to the value from Zhang10, MERRA, and CFSR) may be related to the changes in samples of stations in SON to satisfy the bare land or sparsely vegetated conditions in addition to the scale discrepancy between the points and grids which varies as the sample changes.

The seasonal and annual anomalies of latent and sensible heat fluxes averaged over CMA stations from the fused data were compared with those from reanalysis, remote sensing, and Yang11 datasets (Figs. 4 and 5). Because no direct measurement of the latent and sensible heat fluxes was possible over the CMA stations, the accuracy of the variation and trend from Yang11 could not be validated directly as was only compared with other datasets. Although the interannual variability of the latent heat flux in MAM and DJF and the sensible heat flux in all seasons except JJA from CFSR were larger than those of other datasets, all datasets showed consistent variation of latent heat flux in SON and sensible heat flux in JJA when the decadal changes were most significant. The season with the weakest Pearson correlation of the sensible/latent heat flux between the fused data and Yang11 was MAM, when divergences of anomalies among reanalysis, remote sensing, and Yang11 were present. The potential causes of this phenomenon may include the weak correlation of albedo (−0.15) and net radiation (−0.02) between the fused net radiation and Yang11 (result not shown); the large uncertainty in modeling the SEB in MAM, as indicated from the wide variety of multiple datasets; and the heterogeneity and physical effects such as soil moisture and albedo from snow cover changes. All datasets except MERRA showed a weak tendency of sensible heat flux annually and in JJA and SON; however, the magnitudes differed (Table 6). Such consistent tendency of SEB changes has the potential for inferring the feedback of SEB under the framework of climate change (Andrews et al., 2009; Richardson et al., 2013). In contrast to the continuous intensified tendency of the latent heat flux from Yang11 in MAM, Zhang10 and the fused dataset resembled a pattern similar to that from a global study that indicated a transition from increasing to decreasing in the late 1990s (Jung et al., 2010). The most significant decadal changes of the latent heat flux occurred in SON, when fused datasets, all reanalysis datasets except MERRA and Yang11 showed an increasing tendency that ranged from $1.1\,\mathrm{W\,m^{-2}\,decade^{-1}}$ to $2.9\,\mathrm{W\,m^{-2}\,decade^{-1}}$. This is probably related to the modeling errors in SON when the model used in Yang11 produces too high latent heat flux (K. Yang, personal communication, 2013). Overall, the fused datasets displayed the highest accuracy according to cross-validation in addition to a consistent seasonal cycle with that from Yang09, which is described in the following sections.

4.3 Spatiotemporal characterization of sensible heat flux

In contrast to the seasonal evolution of the latent heat flux, the sensible heat flux was lower in JJA than that in MAM in the eastern TP, corresponding to the onset of the summer monsoon, as illustrated in Fig. 6. The sensible heat flux reached the lowest value in DJF and decreased with latitude. In MAM, JJA, and SON, the high values were located in the northern mountains and basins, the center of the western plateau, and the Himalaya ranges in the south TP, respectively. The annual STD was high in most dry area, including the northern ranges and basin and in the center of the western plateau. The high STD area formed in the center of the western plateau in JJA and moved to the northern ranges in SON. The southeastern TP had a low STD in all seasons. The annual pattern of the decadal changes of sensible heat flux reflects the increases of sensible heat flux in the western TP in MAM and JJA and the decrease of sensible heat flux in JJA and SON. Therefore, the weakening of JJA and annual sensible heat flux

ACPD
13, 30349–30405, 2013

is consistent with the observed decrease of sensible heat flux, wind stilling, and solar dimming from CMA stations over the TP (Tang et al., 2011; Yang et al., 2011c).

The temporal variations of sensible heat flux averaged over the TP correlated to cloud cover, water vapor, temperature anomalies, snow cover, and net radiative fluxes (Table 7). The sensible heat flux anomalies correlated to the variations in the net shortwave or all-wave net radiation in all seasons, with the correlation coefficient reaching the maximum in MAM. Thus, the following analysis focuses on cloud cover and water vapor, which are the two dominant factors that regulate the surface radiation budget and have the potential to be regulated by the feedback from local sensible heat fluxes (Shi and Liang, 2013a). The axis of cloud cover and water vapor in Fig. 7 is reversed to facilitate visual interpretation. The negative correlation between annual cloud cover and sensible heat flux was stronger than that from each season, which corresponding to the dominant role of cloud cover in regulating downward shortwave irradiance and net radiation. Positive correlation between the sensible heat flux and water vapor/temperature existed only in MAM, when major peaks of sensible heat flux were consistent with that from water vapor in 1990, 1993, and 2004. In JJA, the weakening of the sensible heat flux by $-3.9\,\mathrm{W\,m^{-2}\,decade^{-1}}$ is coincident with the increase of water vapor and cloud cover, and the interannual variability is negatively correlated to that from water vapor and cloud cover by −0.52 and −0.39, respectively. The correlation between the sensible heat flux and temperature over the TP suggests two possible physical links: the sensible heat flux mainly warms the surface air in MAM as indicated from the positive correlation with mean temperature, and it is suppressed from the weakened temperature gradient in JJA and SON, as suggested from the negative (positive) correlation to mean temperature (temperature range).

4.4 Spatiotemporal characterization of latent heat flux

The seasonal and annual mean, STD, and decadal changes of the fused latent heat flux over the TP from 1984 to 2007 are shown in Fig. 8. The latent heat flux increased from northwest to southeast over the TP in all seasons. In JJA, the high mean value area

ACPD
13, 30349–30405, 2013

was located in the east TP and in the southwest boundaries. STD was high (low) in the center of the western plateau in JJA (MAM). The annual STD is similar to that in SON with high and low values in the center eastern and northern ranges of TP, respectively. The northeastern (northwestern) TP experience increased (decreased) latent heat flux in all seasons with a maximum value in JJA. A significantly decreased latent heat flux was located in areas over the southern ranges and valleys in MAM and JJA. In general, the climatology of mean and STD of latent heat flux corresponded to the elevation from the northwestern to southeastern TP and to the dry and wet climate in the western and eastern TP. The decadal changes of latent heat flux indicate a contrasting effect with suppressed (intensified) hydrological cycles in high (low) latent heat flux areas except for the northwestern TP region, where large uncertainties may be existed since no ground observation is available to calibrate the fused data sets over the western TP.

The interannual variation of the latent heat flux over the TP has been compared with atmospheric and surface conditions and surface net radiative fluxes that may regulate the latent heat flux (Wang and Liang, 2008; Wang and Dickinson, 2012). Considering the data dependency (such that GIMMS NDVI is used as an input for Zhang10), several significantly correlated surface variables (mean temperature; temperature range; maximum temperature, and snow cover) are reported in Table 6 and the latent heat flux anomalies are only plotted with cloud cover and water vapor anomalies. The latent heat flux decreased (increased) significantly in MAM (SON) in recent decades by $-0.7\,\mathrm{W\,m^{-2}\,decade^{-1}}$ ($1.0\,\mathrm{W\,m^{-2}\,decade^{-1}}$) (Table 6). The annual latent heat flux displayed a transition from increasing to decreasing in the late 1990s, coincident with the transition to the positive water vapor anomalies observed from 1997 to 1998 (Yang et al., 2011c). This phenomenon is possibly attributed to the inclusion of the Geostationary Meteorological Satellite (GMS) as inputs in reanalysis and remote sensing SEB retrieval, whereas no GMS observation is available over the TP before the late 1990s (Oku et al., 2007). In SON and DJF, interannual variation correlated strongly to that from water vapor (Fig. 9), with correlation coefficients of 0.85 and 0.65, respectively (Table 7). In MAM, a similar pattern of anomalies existed among latent heat flux, cloud

ACPD
13, 30349–30405, 2013

cover, and water vapor from 1995 to 2003, whereas opposite variations dominated between latent heat flux and water vapor before 1995 and after 2003. The seasonal variation of latent heat flux was inherited from the NDVI anomalies as input to the Zhang10 with highest R^2 in JJA of 0.73, suggesting the importance of vegetation for regulating regional latent heat flux during the growing seasons. The weak correlation between the cloud cover/water vapor and latent heat flux in JJA indicates a potential change in the dominant physical mechanism that determines the variation of latent heat flux from other seasons according to such factors as cloud depth or duration, wind speed, solar irradiance, and vegetation conditions. In general, the latent heat flux anomalies are likely most associated with interannual variation of cloud cover (except in MAM) and water vapor, which is related to the surface water vapor pressure and moisture feedbacks to the atmosphere, whereas the maximum temperature and soil moisture (relative to the temperature range) act only as significant factors for latent heat flux anomalies in SON and at the annual scale, respectively.

Attentions should be paid when interpreting the decadal changes of the fused latent heat flux because of the discrepancy (in magnitude or direction of the trend) among the fused results, ground station retrievals, reanalysis, and remote sensing retrievals (Table 6). Such discrepancy is possibly attributed to the scale mismatch between the pixel area-averages and the point measurements as well as the uncertainties inherited from the data fusion and the ground measurements (Wang and Dickinson, 2012). The fused approach indeed has inferred a spatially heterogeneity in the decadal changes of the latent heat flux over the TP, which could not be derived using in situ retrievals along and is most consistent to the input reanalysis or remote sensing datasets with large assigned coefficients (i.e., ERA-Interim and Zhang10) as shown in Table 4 (result not shown). The decreased latent heat flux over the southeastern TP (the center TP) in spring (summer) is likely related to the decreased precipitation because of the weakened monsoon (suppressed potential evaportranspiration) in recent decades (Zhou and Huang, 2012; Lei et al., 2013). Due to the extreme-sparse in situ observations and the lack of varied long-term remote sensing products, further investigations are encouraged to verify the confidence of the fused data in representing the actual decadal changes by comparing to other independent observational datasets (i.e., remote sensing observations and ground observations) in future studies, especially over the western TP where large uncertainties could impact the fidelity of the trend.

5 Discussions

5.1 The energy balance closure issue

The residue of the SEB at stations over the TP is likely originated from measuring error, sampling mismatch, soil energy storage, advection, and large scale eddies from heterogeneity (Li et al., 2005; Foken et al., 2006; Foken, 2008). Measurements are mounted at different heights with substantially different footprint at each station, which requires stability and surface homogeneity to close the SEB. In addition, systematic and random errors from in situ measurement have been argued as causes for the SEB imbalance through overestimation (underestimation) of latent and sensible heat fluxes (net radiation). Specifically, analysis from previous studies and high residue error in JJA from the current study suggest that the systematic error from the infrared hygrometer is critical to the closure problem, particularly during rainfall days, which is associated with lower latent heat flux from weakened measured fluctuation of specific humidity (Tanaka et al., 2003; Yang et al., 2004). In addition, the freezing and thawing season is related to variation in closure ratio (CR in Eq. 3), which reaches a negative value in the completely frozen stage (Guo et al., 2011a). Although no agreements or protocols has been reached for the causes and corrections of energy balance and imbalance from eddy covariance measurement over the TP, closure of the SEB on the daily scale limits the effect of imbalance from diurnal variation, such as that through the freezing and melting processes and the energy storage from photosynthesis of plants, by calculating the daily average (Tanaka et al., 2003; Yang et al., 2004; Yang and Koike, 2008; Guo et al., 2011a). Extensive eddy covariance measurements in various climatic regions and land cover types over the TP are required in future research to quantify conditions under which the energy budget is unbalanced.

$$CR = \frac{[(NR - G) - (LE + H)]}{(NR - G)} \quad (3)$$

5.2 Uncertainties of the fused surface energy fluxes

5.2.1 Input error

The varied accuracies constraints from inputs and methods by which the latent and sensible heat fluxes are estimated complicate the quality assessment of the SEB from stations, reanalysis, and remote sensing datasets. Specifically, the input error of the fused SEB is referred to as errors from the monthly value for ground-measured, reanalysis, or remote sensing datasets. Previous studies suggest that no single reanalysis dataset is superior to others in terms of routinely measured surface variables such as temperature, precipitation, humidity, pressure, and wind speed and the surface radiation budget, which suggests divergent representation and parameterization of the diurnal cycles of surface variables such as ground–air temperature, wind speed, and aerodynamic roughness in the land surface models used to estimate the SEB (Wang and Zeng, 2012; Zhu et al., 2012). The uncertainty from Zhang10 could be inherited through errors from the AVHRR GIMMS NDVI as inputs and the energy imbalance of eddy covariance measurements as training samples (Zhang et al., 2010). Additional dominant input error is sourced from net radiation and downward shortwave irradiance, which largely determine the available energy to be partitioned into heat fluxes (Liang et al., 2013). The validation result also proves that accuracy of the latent heat flux is significantly higher than the sensible heat flux from reanalysis or remote sensing, which is largely attributed to the coherent constraints of the latent heat flux from hydrological cycles and the surface energy balance, which improve estimations of precipitation and net radiation, respectively, over the TP (Mueller et al., 2013).

ACPD
13, 30349–30405, 2013

5.2.2 Error propagation

The uncertainty of the fused SEB is affected by error propagation through calculations, including eddy-covariance retrieval, threshold filtering, averaging, interpolation, and data fusion. The present study takes advantage of both well-characterized variables in term of RMSEs of remote sensing and reanalysis datasets and addition/subtraction rather than multiplication/division according to the physically based surface energy balance (Eq. 1) to constrain the uncertainty of the fused sensible heat flux. For instance, the error propagation largely limited an alternative way to apply MLR to both sensible and latent heat flux and adjusted to close Bowen ratio (Fusion, MLR close Bowen ratio in Table 5). It is worth noting that eddy-covariance retrieval and MLR data fusion employ both multiplication and addition/subtraction, suggesting that uncertainty of the fused SEB could be amplified from those calculations. Nevertheless, the data fused approach is an applicable method for this regional application because it has fewer uncertainties associated with error propagation than that by using land surface modeling, which requires significant amounts of input, parameterization, and nonlinear modeling (Wang and Dickinson, 2012).

5.2.3 Resample scale

The error of the fused data introduced by the resample scale is an emergent issue in the case of integrating synthesis that uses multiple datasets at various spatial resolutions. The impact of the resample scale has been assessed by applying the proposed data fusion method to seven grid sizes including 0.1°, 0.3°, 0.5°, 1.0°, 1.5°, 2.0°, and 2.5° to compare the sensitivity to the resample scale among the fused, reanalysis, and remote sensing datasets (Fig. 10). The RMSE_CV of the ground heat flux and the sensible heat flux is less variable than that of the latent heat flux among the various scales, which supports the expectation of higher heterogeneity of latent heat flux and the potential for different footprint to exist for latent and sensible heat fluxes (Kustas et al., 2006; Ma et al., 2006). In addition, the robustness of fused latent and sensible

Discussion Paper | Discussion Paper | Discussion Paper | Discussion Paper |

ACPD
13, 30349–30405, 2013

Surface sensible and latent heat fluxes over the Tibetan Plateau

Q. Shi and S. Liang

heat fluxes is supported more by lower variation in RMSE_CV with the decreased resample scale than by reanalysis and remote sensing datasets. The magnitude of the changes in RMSE_CV ($\pm 2.5\,\mathrm{W\,m^{-2}}$) resulting from the various resample scales below 1.5° was less than that from the instrumental errors introduced in Sect. 2.1.

5.2.4 Data fusion method

In the case of high-level data fusion for the SEB, such as feature-level image fusion according to Pohl and Van Genderen (1998), the MLR fused method constrains the error of the fused SEB through minimization of the residue error. To quantify the potential error from the selection of the data fusion method, experiments have been conducted in which the same inputs were used for different linear regression models, including stepwise regression, which selects datasets by excluding those from the starting model to minimize the Bayesian information criterion (BIC); principle analysis regression (PCA), which inherits from the MLR but uses the first two or three principle components of input datasets (PCA_2 and PCA_3); and adapted lasso regression, which improves the lasso regularization technique in the selection of datasets to simultaneously estimate and select variables with adaptive weights (Zou, 2006). Advanced statistical methods with the potential for revealing unseen (i.e., nonlinear) processes by linear approximations were selected for comparison with the MLR results, including Supported Vector Regression (SVM) (Vapnik, 1999) and Random Forest (RF) regression (Breiman, 2001). SVM computes optimized hyperplanes that maximize the deviations from the targets, which has been applied in the fusing of multiple remote sensing datasets in cases such fuel mapping and precipitation retrievals (García et al., 2011; Wei and Roan, 2012). RF realizes the concept of ensemble learning from the group of regression trees through processes of boosting and bagging. An additional commonly used method, particularly in multi-model fusion, is Bayesian model averaging (BMA), which was implemented to optimize weights to integrate predictive distributions from multi-models such as the mapping of longwave radiative fluxes from multiple models (Raftery et al., 2005; Wu et al., 2012b). Overall, the largest absolute differences in RMSE_CV of latent and sensible heat fluxes

ACPD
13, 30349–30405, 2013

between the MLR and other linear regression models are relatively low, by 1.4 $\mathrm{W\,m^{-2}}$ and 0.9 $\mathrm{W\,m^{-2}}$, respectively, with respect to that from the various resample scales and documented instrument uncertainties. MLR outperformed those from SVM, RF, and BMA, indicating that the MLR model can effectively achieve the goal of data integration in this study. Moreover, the limited accuracy improved by the three advanced models could be attributed to the extreme limited capability of the training stations to approximate true-state statistics. Because the presented comparisons of various data fusion methods are empirical and do not include modeling, comparisons of the results with those from data assimilation techniques have not been conducted in this study and remain a key topics for future research.

5.3 Implications for land–biosphere–atmosphere interactions and climate change

The fused sensible and latent heat fluxes prompt interest in understanding the changes in land–biosphere–atmosphere interactions over the TP. Applying remote sensing observations in land surface modeling enables the quantification of the SEB at the spatial continuous scale to be extended to the satellite era over two decades, which is otherwise impossible when using ground observations at the footprint scale alone (Pinker, 1990). In JJA, the observed solar dimming limits the available net radiation, possibly resulting in the weakening of the sensible heat flux, which further constrains the atmospheric circulation pattern. However, the latent heat flux from dry (wet) regions responds to the reduction of net radiation in JJA with increased (decreased) values indicate that vegetation may modulate the strength of the JJA transpiration and soil evaporation through nonuniform changes in physiological activities such as stomata openings and microclimate conditions such as temperature gradient, wind, and soil moisture (Wild, 2012; You et al., 2013; Richardson et al., 2013). The seasonal dependence, as indicated from the correlation among surface sensible/latent heat flux and cloud cover, water vapor, temperature, and temperature range suggests that regional land–biosphere–atmosphere interactions may be associated with the advance and retreat of the summer and winter monsoon climates. The mechanisms by which land–biosphere–atmosphere interactions mitigate or amplify the changes of the surface latent and sensible heat flux over the TP have received little attention; therefore, future investigation should address this challenge by using models capable of reproducing past climate changes and variation of the surface heat fluxes over the TP.

6 Conclusions

The spatiotemporal characterization of the surface sensible and latent heat fluxes over the TP covering the period from 1984 to 2007 is presented by using the fused monthly latent and sensible heat fluxes at 0.5° from ground-measured datasets including AsiaFlux, ChinaFLUX, GAME/Tibet, and CAMP/Tibet; the Zhang10 remote sensing dataset; and reanalysis datasets including CFSR, MERRA, ERA-Interim, and JRA-25. The surface sensible and latent heat fluxes from reanalysis and remote sensing datasets were first validated against those from ground measurement at the monthly scale and were next synthesized by using the multiple linear regression approach. The energy balance was closed at the daily scale to reduce uncertainties evolving in the diurnal cycles over the TP stations. The uncertainties of the fused surface sensible and latent heat fluxes were discussed from various aspects in which uncertainties propagating from input errors and instrumental errors were likely the dominant factors when comparing with that from the interpolation scale and the selection of the fusion method. Results from the leave-one-site-out cross-validation suggest that the fused monthly latent and sensible heat fluxes had the lowest RMSE_CVs, at 11.1 $\mathrm{W\,m^{-2}}$ and 16.4 $\mathrm{W\,m^{-2}}$, respectively, against those using each calibrated dataset. In addition, the fused sensible heat flux consistently captured the monthly cycle to the datasets by using only meteorological observations at CMA sites (Yang09).

At the regional scale, the latent and sensible heat fluxes displayed different seasonal evolution and distribution patterns, which are likely associated with latitudinal gradient,

ACPD
13, 30349–30405, 2013

elevation difference, and monsoon climate over the TP. The highest value area of latent heat flux was located in the east TP and the south face of the southwest ranges, which are largely affected by the summer monsoon, whereas the sensible heat flux was high the middle-northern ranges, which are dry in MAM and JJA. Over the recent two decades, the spatial pattern of the decadal changes in the sensible heat flux has been dominated by a continuous decrease in most areas in JJA and SON and an increasing tendency in the western TP, which is consistent with the observed solar dimming and weakened sensible heat flux at the station scale over the TP (Yang et al., 2011b; You et al., 2013). On the contrary, the latent heat flux exhibited a significant but weaker trend and a more fragmented pattern than that from the sensible heat flux with an increase in the northeastern TP in all seasons and decreases in the outer areas of the western and eastern TP in MAM and JJA. The derived spatial pattern of decadal changes of the sensible and latent heat flux requires further validation over the western TP since uncertainties could be very large over area without any calibration sites.

The interannual anomalies of the latent and sensible heat fluxes averaged over the TP were explained through Pearson correlation analysis including such factors as cloud cover, water vapor, NDVI, snow cover, temperature, maximum temperature, and temperature range. A strong correlation between latent heat flux and water vapor existed in SON and DJF, whereas a strong high correlation to sensible heat flux existed in MAM and JJA but in opposite directions. During MAM and SON, in which the most significant trends existed for the sensible and latent heat fluxes, respectively, the number of significant correlated variables was the largest, and the magnitude of most correlations was the largest of all seasons. These results imply that the coherent changes in the surface and atmospheric variables could relate to decadal changes over the TP by influencing the surface radiation budget, transpiration (evaporation) of vegetation (soil), or temperature gradient. Such results confirm that land–biosphere–atmosphere interactions may regulate the temporal variation of the surface sensible and latent heat fluxes, although the magnitude of such couplings has seasonal dependence. Because approximately one-fourth of the world's population is affected by the East Asian monsoon, which is

ACPD
13, 30349–30405, 2013

fueled by sensible and latent heat fluxes over the TP, it would be interesting to quantify the drivers and responses of the changes in surface sensible and latent heat fluxes in future research by using numerical modeling.

Acknowledgements. This study is funded by the National Oceanic and Atmospheric Administration (NOAA). We are grateful to researchers from AsiaFlux, ChinaFLUX, GAME/Tibet, CEOP/Tibet, and NMIC/CMA for providing ground observation data over the TP. The CFSR and JRA data are from the Research Data Archive (RDA), which is maintained by the Computational and Information Systems Laboratory (CISL) at the National Center for Atmospheric Research (NCAR). We thank the Global Modeling and Assimilation Office (GMAO) and the GES DISC for the dissemination of MERRA, ECMWF data server for ERA Interim, and the University of Montana Numerical Terradynamic Simulation Group for Zhang10. We acknowledge researchers from the Princeton University terrestrial hydrology research group for proving the PU-ET, NASA Global Inventory Modeling and Mapping Studies (GIMMS) for providing the AVHRR GIMMS NDVI, the British Atmospheric Data Centre (BADC) for providing CRU TS3.1 temperature and cloud cover, and the Rutgers University Global Snow Lab for providing Northern Hemisphere snow cover. The GLDAS data are acquired as part of a mission of NASA's Earth Science Division and archived and distributed by the Goddard Earth Sciences (GES) Data and Information Services Center (DISC), NRA-1 and NRA-2 are from the NOAA/OAR/ESRL PSD. A special thanks to Kun Yang who has provided not only Yang09 and Yang11 datasets and but also constructive comments. We thank Martin Jung (Max Planck Institute for Biogeochemistry) and Joshua Fisher (NASA Jet Propulsion Laboratory) for the provision of MPI-LE-H and PU-LE.

References

An, Z., Kutzbach, J. E., Prell, W. L., and Porter, S. C.: Evolution of Asian monsoons and phased uplift of the Himalaya–Tibetan Plateau since Late Miocene times, Nature, 411, 62, doi:10.1038/35075035, 2001.

Andrews, T., Forster, P. M., and Gregory, J. M.: A surface energy perspective on climate change, J. Climate, 22, 2557–2570, doi:10.1175/2008jcli2759.1, 2009.

Baldocchi, D., Falge, E., Gu, L., Olson, R., Hollinger, D., Running, S., Anthoni, P., Bernhofer, C., Davis, K., Evans, R., Fuentes, J., Goldstein, A., Katul, G., Law, B., Lee, X., Malhi, Y., Meyers, T., Munger, W., Oechel, W., Paw, K. T., Pilegaard, K., Schmid, H. P., Valentini, R., Verma, S., Vesala, T., Wilson, K., and Wofsy, S.: FLUXNET: a new tool to study the temporal and spatial variability of ecosystem-scale carbon dioxide, water vapor, and energy flux densities, B. Am. Meteorol. Soc., 82, 2415–2434, doi:10.1175/1520-0477(2001)082<2415:FANTTS>2.3.CO;2, 2001.

Bian, L., Gao, Z., Ma, Y., Koike, T., Ma, Y., Li, Y., Sun, J., Hu, Z., and Xu, X.: Seasonal variation in turbulent fluxes over Tibetan Plateau and its surrounding areas: research note, J. Meteorol. Soc. Jpn., 90C, 157–171, doi:10.2151/jmsj.2012-C11, 2012.

Breiman, L.: Random Forests, Mach. Learn., 45, 5–32, doi:10.1023/a:1010933404324, 2001.

Chen, F., Janjić, Z., and Mitchell, K.: Impact of atmospheric surface-layer parameterizations in the new land-surface scheme of the NCEP Mesoscale Eta Model, Bound.-Lay. Meteorol., 85, 391–421, doi:10.1023/a:1000531001463, 1997.

Chen, X., Su, Z., Ma, Y., and Sun, F.: Analysis of land-atmosphere interactions over the north region of Mt. Qomolangma (Mt. Everest), Arct. Antarct. Alp. Res., 44, 412–422, doi:10.1657/1938-4246-44.4.412, 2012.

Chen, X., Su, Z., Ma, Y., Yang, K., and Wang, B.: Estimation of surface energy fluxes under complex terrain of Mt. Qomolangma over the Tibetan Plateau, Hydrol. Earth Syst. Sci., 17, 1607–1618, doi:10.5194/hess-17-1607-2013, 2013a.

Chen, X., Su, Z., Ma, Y., Yang, K., Wen, J., and Zhang, Y.: An improvement of roughness height parameterization of the Surface Energy Balance System (SEBS) over the Tibetan Plateau, J. Appl. Meteorol. Clim., 52, 607–622, doi:10.1175/jamc-d-12-056.1, 2013b.

Chen, Y., Yang, K., Zhou, D., Qin, J., and Guo, X.: Improving the Noah land surface model in arid regions with an appropriate parameterization of the thermal roughness length, J. Hydrometeorol., 11, 995–1006, doi:10.1175/2010jhm1185.1, 2010.

Dee, D., Uppala, S. M., Simmons, A. J., Berrisford, P., Poli, P., Kobayashi, S., Andrae, U., Balmaseda, M. A., Balsamo, G., Bauer, P., Bechtold, P., Beljaars, A. C. M., van de Berg, L., Bidlot, J., Bormann, N., Delsol, C., Dragani, R., Fuentes, M., Geer, A. J., Haimberger, L., Healy, S. B., Hersbach, H., Hólm, E. V., Isaksen, L., Kållberg, P., Köhler, M., Matricardi, M., McNally, A. P., Monge-Sanz, B. M., Morcrette, J. J., Park, B. K., Peubey, C., de Rosnay, P., Tavolato, C., Thépaut, J. N., and Vitart, F.: The ERA-Interim reanalysis: configuration and performance of the data assimilation system, Q. J. Meteor. Soc., 137, 553–597, doi:10.1002/qj.828, 2011.

ACPD
13, 30349–30405, 2013

Douville, H., Royer, J. F., and Mahfouf, J. F.: A new snow parameterization for the Météo-France climate model, Clim. Dynam., 12, 21–35, doi:10.1007/bf00208760, 1995.
Douville, H., Viterbo, P., Mahfouf, J.-F., and Beljaars, A. C. M.: Evaluation of the optimum interpolation and nudging techniques for soil moisture analysis using FIFE data, Mon. Weather Rev., 128, 1733–1756, doi:10.1175/1520-0493(2000)128<1733:eotoia>2.0.co;2, 2000.
Duan, A., Wang, M., Lei, Y., and Cui, Y.: Trends in summer rainfall over China associated with the Tibetan Plateau sensible heat source during 1980–2008, J. Climate, 26, 261–275, doi:10.1175/jcli-d-11-00669.1, 2013.
Ek, M. B., Mitchell, K. E., Lin, Y., Rogers, E., Grunmann, P., Koren, V., Gayno, G., and Tarpley, J. D.: Implementation of Noah land surface model advances in the National Centers for Environmental Prediction operational mesoscale Eta model, J. Geophys. Res.-Atmos., 108, 8851, doi:10.1029/2002jd003296, 2003.
Foken, T.: The energy balance closure problem: an overview, Ecol. Appl., 18, 1351–1367, 2008.
Foken, T., Wimmer, F., Mauder, M., Thomas, C., and Liebethal, C.: Some aspects of the energy balance closure problem, Atmos. Chem. Phys., 6, 4395–4402, doi:10.5194/acp-6-4395-2006, 2006.
García, M., Riaño, D., Chuvieco, E., Salas, J., and Danson, F. M.: Multispectral and LiDAR data fusion for fuel type mapping using support vector machine and decision rules, Remote Sens. Environ., 115, 1369–1379, doi:10.1016/j.rse.2011.01.017, 2011.
Gu, S., Tang, Y. H., Cui, X. Y., Kato, T., Du, M. Y., Li, Y. N., and Zhao, X. Q.: Energy exchange between the atmosphere and a meadow ecosystem on the Qinghai–Tibetan Plateau, Agr. Forest Meteorol., 129, 175–185, doi:10.1016/j.agrformet.2004.12.002, 2005.
Guo, D., Yang, M., and Wang, H.: Characteristics of land surface heat and water exchange under different soil freeze/thaw conditions over the central Tibetan Plateau, Hydrol. Process., 25, 2531–2541, doi:10.1002/hyp.8025, 2011a.
Guo, X., Yang, K., and Chen, Y.: Weakening sensible heat source over the Tibetan Plateau revisited: effects of the land–atmosphere thermal coupling, Theor. Appl. Climatol., 104, 1–12, doi:10.1007/s00704-010-0328-1, 2011b.
Immerzeel, W. W., van Beek, L. P. H., and Bierkens, M. F. P.: Climate change will affect the Asian water towers, Science, 328, 1382–1385, doi:10.1126/science.1183188, 2010.

Jiménez, C., Prigent, C., and Aires, F.: Toward an estimation of global land surface heat fluxes from multisatellite observations, J. Geophys. Res., 114, D06305, doi:10.1029/2008jd011392, 2009.

Jiménez, C., Prigent, C., Mueller, B., Seneviratne, S. I., McCabe, M. F., Wood, E. F., Rossow, W. B., Balsamo, G., Betts, A. K., Dirmeyer, P. A., Fisher, J. B., Jung, M., Kanamitsu, M., Reichle, R. H., Reichstein, M., Rodell, M., Sheffield, J., Tu, K., and Wang, K.: Global intercomparison of 12 land surface heat flux estimates, J. Geophys. Res., 116, D02102, doi:10.1029/2010jd014545, 2011.

Jung, M., Reichstein, M., and Bondeau, A.: Towards global empirical upscaling of FLUXNET eddy covariance observations: validation of a model tree ensemble approach using a biosphere model, Biogeosciences, 6, 2001–2013, doi:10.5194/bg-6-2001-2009, 2009.

Jung, M., Reichstein, M., Ciais, P., Seneviratne, S. I., Sheffield, J., Goulden, M. L., Bonan, G., Cescatti, A., Chen, J., de Jeu, R., Dolman, A. J., Eugster, W., Gerten, D., Gianelle, D., Gobron, N., Heinke, J., Kimball, J., Law, B. E., Montagnani, L., Mu, Q., Mueller, B., Oleson, K., Papale, D., Richardson, A. D., Roupsard, O., Running, S., Tomelleri, E., Viovy, N., Weber, U., Williams, C., Wood, E., Zaehle, S., and Zhang, K.: Recent decline in the global land evapotranspiration trend due to limited moisture supply, Nature, 467, 951–954, doi:10.1038/nature09396, 2010.

Jung, M., Reichstein, M., Margolis, H. A., Cescatti, A., Richardson, A. D., Arain, M. A., Arneth, A., Bernhofer, C., Bonal, D., Chen, J., Gianelle, D., Gobron, N., Kiely, G., Kutsch, W., Lasslop, G., Law, B. E., Lindroth, A., Merbold, L., Montagnani, L., Moors, E. J., Papale, D., Sottocornola, M., Vaccari, F., and Williams, C.: Global patterns of land-atmosphere fluxes of carbon dioxide, latent heat, and sensible heat derived from eddy covariance, satellite, and meteorological observations, J. Geophys. Res., 116, G00J07, doi:10.1029/2010jg001566, 2011.

Kalnay, E., Kanamitsu, M., Kistler, R., Collins, W., Deaven, D., Gandin, L., Iredell, M., Saha, S., White, G., Woollen, J., Zhu, Y., Leetmaa, A., Reynolds, R., Chelliah, M., Ebisuzaki, W., Higgins, W., Janowiak, J., Mo, K. C., Ropelewski, C., Wang, J., Jenne, R., and Joseph, D.: The NCEP/NCAR 40-year reanalysis project, B. Am. Meteorol. Soc., 77, 437–471, doi:10.1175/1520-0477(1996)077<0437:tnyrp>2.0.co;2, 1996.

Kiehl, J. T. and Trenberth, K. E.: Earth's annual global mean energy budget, B. Am. Meteorol. Soc., 78, 197–208, doi:10.1175/1520-0477(1997)078<0197:eagmeb>2.0.co;2, 1997.

Kim, J., Miyata, A., and Yu, G.: AsiaFlux-sustaining ecosystems and people through resilience thinking, in: WCC-3 Climate Sense, Tudor Rose, Leicester, UK, 164–168, 2009.
Koike, T.: The Coordinated Enhanced Observing Period – An initial step for integrated global water cycle observation, WMO Bull., 53, 115–121, 2004.
Koster, R. D. and Suarez, M. J.: Energy and water balance calculations in the Mosaic LSM, NASA Tech. Memo. 104606, Vol. 9, 76, NASA Goddard Space Flight Center, Greenbelt, 1996.
Koster, R. D., Suarez, M. J., Ducharne, A., Stieglitz, M., and Kumar, P.: A catchment-based approach to modeling land surface processes in a general circulation model: 1. Model structure, J. Geophys. Res.-Atmos., 105, 24809–24822, doi:10.1029/2000jd900327, 2000.
Kustas, W. P., Anderson, M. C., French, A. N., and Vickers, D.: Using a remote sensing field experiment to investigate flux–footprint relations and flux sampling distributions for tower and aircraft-based observations, Adv. Water Resour., 29, 355–368, doi:10.1016/j.advwatres.2005.05.003, 2006.
Kutzbach, J. E., Prell, W. L., and Ruddiman, W. F.: Sensitivity of Eurasian climate to surface uplift of the Tibetan Plateau, J. Geol., 101, 177–190, doi:10.1086/648215, 1993.
Lee, J. H., Timmermans, J., Su, Z., and Mancini, M.: Calibration of aerodynamic roughness over the Tibetan Plateau with Ensemble Kalman Filter analysed heat flux, Hydrol. Earth Syst. Sci., 16, 4291–4302, doi:10.5194/hess-16-4291-2012, 2012.
Lei, Y., Yao, T., Bird, B. W., Yang, K., Zhai, J., and Sheng, Y.: Coherent lake growth on the central Tibetan Plateau since the 1970s: characterization and attribution, J. Hydrol., 483, 61–67, doi:10.1016/j.jhydrol.2013.01.003, 2013.
Li, Z., Yu, G., Wen, X., Zhang, L., Ren, C., and Fu, Y.: Energy balance closure at ChinaFLUX sites, Sci. China Ser. D., 48, 51–62, 2005.
Liang, S., Wang, K., Zhang, X., and Wild, M.: Review on estimation of land surface radiation and energy budgets from ground measurement, remote sensing and model simulations, IEEE J. Sel. Top. Appl., 3, 225–240, doi:10.1109/JSTARS.2010.2048556, 2010.
Liang, S., Zhao, X., Liu, S., Yuan, W., Cheng, X., Xiao, Z., Zhang, X., Liu, Q., Cheng, J., Tang, H., Qu, Y., Bai, Y., Qu, Y., Ren, H., Yu, K., and Townshend, J.: A long-term Global LAnd Surface Satellite (GLASS) dataset for environmental studies, Int. J. Digit. Earth, doi:10.1080/17538947.2013.805262, in press, 2013.

ACPD
13, 30349–30405, 2013

Liu, S., Li, S.-G., Yu, G.-R., Sun, X.-M., Zhang, L.-M., Hu, Z.-M., Li, Y.-N., and Zhang, X.-Z.: Surface energy exchanges above two grassland ecosystems on the Qinghai-Tibetan Plateau, Biogeosciences Discuss., 6, 9161–9192, doi:10.5194/bgd-6-9161-2009, 2009.

Liu, Y., Wu, G., Hong, J., Dong, B., Duan, A., Bao, Q., and Zhou, L.: Revisiting Asian monsoon formation and change associated with Tibetan Plateau forcing: II. Change, Clim. Dynam., 39, 1183–1195, doi:10.1007/s00382-012-1335-y, 2012.

Ma, W., Ma, Y., Li, M., Hu, Z.g, Zhong, L., Su, Z., Ishikawa, H., and Wang, J.: Estimating surface fluxes over the north Tibetan Plateau area with ASTER imagery, Hydrol. Earth Syst. Sci., 13, 57–67, doi:10.5194/hess-13-57-2009, 2009.

Ma, W., Ma, Y., and Su, B.: Feasibility of retrieving land surface heat fluxes from ASTER data using SEBS: a case study from the NamCo area of the Tibetan Plateau, Arct. Antarct. Alp. Res., 43, 239–245, 2011a.

Ma, Y., Su, Z., Koike, T., Yao, T., Ishikawa, H., Ueno, K., and Menenti, M.: On measuring and remote sensing surface energy partitioning over the Tibetan Plateau – From GAME/Tibet to CAMP/Tibet, Phys. Chem. Earth, 28, 63–74, doi:10.1016/s1474-7065(03)00008-1, 2003.

Ma, Y., Zhong, L., Su, Z., Ishikawa, H., Menenti, M., and Koike, T.: Determination of regional distributions and seasonal variations of land surface heat fluxes from Landsat-7 Enhanced Thematic Mapper data over the central Tibetan Plateau area, J. Geophys. Res., 111, D10305, doi:10.1029/2005jd006742, 2006.

Ma, Y., Zhong, L., Wang, B., Ma, W., Chen, X., and Li, M.: Determination of land surface heat fluxes over heterogeneous landscape of the Tibetan Plateau by using the MODIS and in situ data, Atmos. Chem. Phys., 11, 10461–10469, doi:10.5194/acp-11-10461-2011, 2011b.

Ma, Y., Zhong, L., Wang, Y., and Su, Z.: Using NOAA/AVHRR data to determine regional net radiation and soil heat fluxes over the heterogeneous landscape of the Tibetan Plateau, Int. J. Remote Sens., 33, 4784–4795, doi:10.1080/01431161.2011.638333, 2012.

Manabe, S. and Terpstra, T. B.: The effects of mountains on the general circulation of the atmosphere as identified by numerical experiments, J. Atmos. Sci., 31, 3–42, doi:10.1175/1520-0469(1974)031<0003:TEOMOT>2.0.CO;2, 1974.

Meng, J., Yang, R., Wei, H., Ek, M., Gayno, G., Xie, P., and Mitchell, K.: The land surface analysis in the NCEP Climate Forecast System Reanalysis, J. Hydrometeorol., 13, 1621–1630, doi:10.1175/jhm-d-11-090.1, 2012.

ACPD

13, 30349–30405, 2013

Surface sensible and latent heat fluxes over the Tibetan Plateau

Q. Shi and S. Liang

Title Page
Abstract | Introduction
Conclusions | References
Tables | Figures
◀| |▶
◀ ▶
Back | Close
Full Screen / Esc
Printer-friendly Version
Interactive Discussion

Mitchell, T. D. and Jones, P. D.: An improved method of constructing a database of monthly climate observations and associated high-resolution grids, Int. J. Climatol., 25, 693–712, doi:10.1002/joc.1181, 2005.

Mu, Q., Heinsch, F. A., Zhao, M., and Running, S. W.: Development of a global evapotranspiration algorithm based on MODIS and global meteorology data, Remote Sens. Environ., 111, 519–536, doi:10.1016/j.rse.2007.04.015, 2007.

Mueller, B., Hirschi, M., Jimenez, C., Ciais, P., Dirmeyer, P. A., Dolman, A. J., Fisher, J. B., Jung, M., Ludwig, F., Maignan, F., Miralles, D. G., McCabe, M. F., Reichstein, M., Sheffield, J., Wang, K., Wood, E. F., Zhang, Y., and Seneviratne, S. I.: Benchmark products for land evapotranspiration: LandFlux-EVAL multi-data set synthesis, Hydrol. Earth Syst. Sci., 17, 3707–3720, doi:10.5194/hess-17-3707-2013, 2013.

Oku, Y., Ishikawa, H., and Su, Z.: Estimation of land surface heat fluxes over the Tibetan Plateau using GMS data, J. Appl. Meteorol. Clim., 46, 183–195, doi:10.1175/jam2456.1, 2007.

Oleson, K., Dai, Y., Bonan, G., Bosilovichm, M., Dickinson, R., Dirmeyer, P., Hoffman, F., Houser, P., Levis, S., Niu, G.-Y., Thornton, P., Vertenstein, M., Yang, Z.-L., and Zeng, X.: Technical Description of the Community Land Model (CLM), Tech. Rep. Technical Report NCAR/TN-461 + STR, National Center for Atmospheric Research, Boulder, CO 80307-3000, USA, 2004.

Onogi, K., Tsutsui, J., Koide, H., Sakamoto, M., Kobayashi, S., Hatsushika, H., Matsumoto, T., Yamazaki, N., Kamahori, H., Takahashi, K., Kadokura, S., Wada, K., Kato, K., Oyama, R., Ose, T., Mannoji, N., and Taira, R.: The JRA-25 reanalysis, J. Meteorol. Soc. Jpn., 85, 369–432, doi:10.2151/jmsj.85.369, 2007.

Pinker, R. T.: Satellites and our understanding of the surface energy balance, Palaeogeogr. Palaeoecol., 82, 321–342, doi:10.1016/S0031-0182(12)80007-1, 1990.

Pinker, R. T. and Ewing, J. A.: Modeling surface solar radiation: model formulation and validation, J. Clim. Appl. Meteorol., 24, 389–401, doi:10.1175/1520-0450(1985)024<0389:MSSRMF>2.0.CO;2, 1985.

Pinker, R. T. and Laszlo, I.: Modeling surface solar irradiance for satellite applications on a global scale, J. Appl. Meteorol., 31, 194–211, doi:10.1175/1520-0450(1992)031<0194:MSSIFS>2.0.CO;2, 1992.

Pohl, C. and Van Genderen, J. L.: Review article multisensor image fusion in remote sensing: concepts, methods and applications, Int. J. Remote Sens., 19, 823–854, doi:10.1080/014311698215748, 1998.

Qian, Y., Flanner, M. G., Leung, L. R., and Wang, W.: Sensitivity studies on the impacts of Tibetan Plateau snowpack pollution on the Asian hydrological cycle and monsoon climate, Atmos. Chem. Phys., 11, 1929–1948, doi:10.5194/acp-11-1929-2011, 2011.

Raftery, A. E., Gneiting, T., Balabdaoui, F., and Polakowski, M.: Using Bayesian model averaging to calibrate forecast ensembles, Mon. Weather Rev., 133, 1155–1174, doi:10.1175/mwr2906.1, 2005.

Reichle, R. H., Koster, R. D., De Lannoy, G. J. M., Forman, B. A., Liu, Q., Mahanama, S. P. P., and Touré, A.: Assessment and enhancement of MERRA land surface hydrology estimates, J. Climate, 24, 6322–6338, doi:10.1175/jcli-d-10-05033.1, 2011.

Richardson, A. D., Keenan, T. F., Migliavacca, M., Ryu, Y., Sonnentag, O., and Toomey, M.: Climate change, phenology, and phenological control of vegetation feedbacks to the climate system, Agr. Forest Meteorol., 169, 156–173, doi:10.1016/j.agrformet.2012.09.012, 2013.

Rienecker, M. M., Suarez, M. J., Gelaro, R., Todling, R., Bacmeister, J., Liu, E., Bosilovich, M. G., Schubert, S. D., Takacs, L., Kim, G.-K., Bloom, S., Chen, J., Collins, D., Conaty, A., da Silva, A., Gu, W., Joiner, J., Koster, R. D., Lucchesi, R., Molod, A., Owens, T., Pawson, S., Pegion, P., Redder, C. R., Reichle, R., Robertson, F. R., Ruddick, A. G., Sienkiewicz, M., and Woollen, J.: MERRA: NASAs Modern-Era Retrospective analysis for Research and Applications, J. Climate, 24, 3624–3648, doi:10.1175/JCLI-D-11-00015.1, 2011.

Robinson, D. A., Dewey, K. F., and Heim, R. R.: Global snow cover monitoring: an update, B. Am. Meteorol. Soc., 74, 1689–1696, doi:10.1175/1520-0477(1993)074<1689:gscmau>2.0.co;2, 1993.

Rodell, M., Houser, P. R., Jambor, U., Gottschalck, J., Mitchell, K., Meng, C. J., Arsenault, K., Cosgrove, B., Radakovich, J., Bosilovich, M., Entin*, J. K., Walker, J. P., Lohmann, D., and Toll, D.: The Global Land Data Assimilation System, B. Am. Meteorol. Soc., 85, 381–394, doi:10.1175/BAMS-85-3-381, 2004.

Saha, S., Moorthi, S., Pan, H. L., Behringer, D., Stokes, D., Grumbine, R., Hou, Y. T., Chuang, H. Y., Juang, H. M. H., Sela, J., Iredell, M., Treadon, R., Keyser, D., Derber, J., Ek, M., Lord, S., Van Den Dool, H., Kumar, A., Wang, W., Long, C., Chelliah, M., Xue, Y., Schemm, J. K., Ebisuzaki, W., Xie, P., Higgins, W., Chen, Y., Wu, X., Wang, J., Nadiga, S., Kistler, R., Woollen, J., Liu, H., Gayno, G., Kleist, D., Van Delst, P., Meng, J., Wei, H., Yang, R., Chen, M., Zou, C. Z., Han, Y., Cucurull, L., Goldberg, M., Liu, Q., Rutledge, G., Tripp, P., Reynolds, R. W., Huang, B., Lin, R., and Zhou, S.: The NCEP climate forecast system reanalysis, B. Am. Meteorol. Soc., 91, 1015–1057, doi:10.1175/2010BAMS3001.2, 2010.

Sato, N., Sellers, P. J., Randall, D. A., Schneider, E. K., Shukla, J., Kinter, J. L., Hou, Y. T., and Albertazzi, E.: Effects of implementing the Simple Biosphere Model in a general circulation model, J. Atmos. Sci., 46, 2757–2782, doi:10.1175/1520-0469(1989)046<2757:eoitsb>2.0.co;2, 1989.

Sellers, P. J., Mintz, Y., Sud, Y. C., and Dalcher, A.: A Simple Biosphere Model (SIB) for use within general circulation models, J. Atmos. Sci., 43, 505–531, doi:10.1175/1520-0469(1986)043<0505:asbmfu>2.0.co;2, 1986.

Sellers, P. J., Randall, D. A., Collatz, G. J., Berry, J. A., Field, C. B., Dazlich, D. A., Zhang, C., Collelo, G. D., and Bounoua, L.: A revised land surface parameterization (SiB2) for atmospheric GCMS. Part I: Model formulation, J. Climate, 9, 676–705, doi:10.1175/1520-0442(1996)009<0676:arlspf>2.0.co;2, 1996.

Shi, Q. and Liang, S.: Characterizing the surface radiation budget over the Tibetan Plateau with ground-measured, reanalysis, and remote sensing data sets: 1. Methodology, J. Geophys. Res.-Atmos., 118, 9642–9657, doi:10.1002/jgrd.50720, 2013a.

Shi, Q. and Liang, S.: Characterizing the surface radiation budget over the Tibetan Plateau with ground-measured, reanalysis, and remote sensing data sets: 2. Spatiotemporal analysis, J. Geophys. Res.-Atmos., 118, 8921–8934, doi:10.1002/jgrd.50719, 2013b.

Stephens, G. L., Li, J., Wild, M., Clayson, C. A., Loeb, N., Kato, S., L'Ecuyer, T., Stackhouse, P. W., Lebsock, M., and Andrews, T.: An update on Earth's energy balance in light of the latest global observations, Nat. Geosci., 5, 691–696, doi:10.1038/ngeo1580, 2012.

Stevens, B. and Schwartz, S.: Observing and modeling Earth's energy flows, Surv. Geophys., 33, 779–816, doi:10.1007/s10712-012-9184-0, 2012.

Stieglitz, M., Ducharne, A., Koster, R., and Suarez, M.: The impact of detailed snow physics on the simulation of snow cover and subsurface thermodynamics at continental scales, J. Hydrometeorol., 2, 228–242, doi:10.1175/1525-7541(2001)002<0228:tiodsp>2.0.co;2, 2001.

Sugita, M., Nohara, D., Miyazaki, S., Yamanaka, T., Kimura, F., and Yasunari, T.: GAME Asian Automatic Weather Station Network (AAN) Data Set Version 3.0, available at the AAN Data Center at: http://www.suiri.tsukuba.ac.jp/Project/aan/aan.html (last access: 8 July 2013) and on GAME CD-ROM No. 13, GAME AAN Working Group Office, Terrestrial Environment Research Center, University of Tsukuba, Tsukuba, Ibaraki, Japan, 2005.

Tanaka, K., Tamagawa, I., Ishikawa, H., Ma, Y., and Hu, Z.: Surface energy budget and closure of the eastern Tibetan Plateau during the GAME-Tibet IOP 1998, J. Hydrol., 283, 169–183, doi:10.1016/s0022-1694(03)00243-9, 2003.

Tang, W.-J., Yang, K., Qin, J., Cheng, C. C. K., and He, J.: Solar radiation trend across China in recent decades: a revisit with quality-controlled data, Atmos. Chem. Phys., 11, 393–406, doi:10.5194/acp-11-393-2011, 2011.

Trenberth, K. E., Fasullo, J. T., and Kiehl, J.: Earth's global energy budget, B. Am. Meteorol. Soc., 90, 311–323, doi:10.1175/2008bams2634.1, 2009.

Tucker, C. J., Pinzon, J. E., Brown, M. E., Slayback, D. A., Pak, E. W., Mahoney, R., Vermote, E. F., and El Saleous, N.: An extended AVHRR 8-km NDVI dataset compatible with MODIS and SPOT vegetation NDVI data, Int. J. Remote Sens., 26, 4485–4498, doi:10.1080/01431160500168686, 2005.

Turner, A. and Slingo, J.: Using idealized snow forcing to test teleconnections with the Indian summer monsoon in the Hadley Centre GCM, Clim. Dynam., 36, 1717–1735, doi:10.1007/s00382-010-0805-3, 2011.

Twine, T. E., Kustas, W. P., Norman, J. M., Cook, D. R., Houser, P. R., Meyers, T. P., Prueger, J. H., Starks, P. J., and Wesely, M. L.: Correcting eddy-covariance flux underestimates over a grassland, Agr. Forest Meteorol., 103, 279–300, doi:10.1016/s0168-1923(00)00123-4, 2000.

Vapnik, V.: The Nature of Statistical Learning Theory, Information Science and Statistics, Springer, New York, 1999.

Vickers, D. and Mahrt, L.: Quality control and flux sampling problems for tower and aircraft data, J. Atmos. Ocean. Tech., 14, 512, doi:10.1175/1520-0426(1997)014<0512:QCAFSP>2.0.CO;2, 1997.

Vinukollu, R. K., Meynadier, R., Sheffield, J., and Wood, E. F.: Multi-model, multi-sensor estimates of global evapotranspiration: climatology, uncertainties and trends, Hydrol. Process., 25, 3993–4010, doi:10.1002/hyp.8393, 2011.

Viterbo, P. and Beljaars, A. C. M.: An improved land surface parameterization scheme in the ECMWF Model and its validation, J. Climate, 8, 2716–2748, doi:10.1175/1520-0442(1995)008<2716:ailsps>2.0.co;2, 1995.

Viterbo, P. and Betts, A. K.: Impact on ECMWF forecasts of changes to the albedo of the boreal forests in the presence of snow, J. Geophys. Res.-Atmos., 104, 27803–27810, doi:10.1029/1998jd200076, 1999.

Wang, A. and Zeng, X.: Evaluation of multireanalysis products with in situ observations over the Tibetan Plateau, J. Geophys. Res., 117, D05102, doi:10.1029/2011jd016553, 2012.
Wang, B., Bao, Q., Hoskins, B., Wu, G., and Liu, Y.: Tibetan Plateau warming and precipitation changes in East Asia, Geophys. Res. Lett., 35, L14702, doi:10.1029/2008gl034330, 2008.
Wang, K. and Dickinson, R. E.: A review of global terrestrial evapotranspiration: observation, modeling, climatology, and climatic variability, Rev. Geophys., 50, RG2005, doi:10.1029/2011RG000373, 2012.
Wang, K. and Liang, S.: An improved method for estimating global evapotranspiration based on satellite determination of surface net radiation, vegetation index, temperature, and soil moisture, J. Hydrometeorol., 9, 712–727, doi:10.1175/2007jhm911.1, 2008.
Wang, Y., Xu, X., Lupo, A. R., Li, P., and Yin, Z.: The remote effect of the Tibetan Plateau on downstream flow in early summer, J. Geophys. Res.-Atmos., 116, D19108, doi:10.1029/2011jd015979, 2011.
Webb, E. K., Pearman, G. I., and Leuning, R.: Correction of flux measurements for density effects due to heat and water vapour transfer, Q. J. Roy. Meteor. Soc., 106, 85–100, doi:10.1002/qj.49710644707, 1980.
Wei, C.-C. and Roan, J.: Retrievals for the rainfall rate over land using special sensor microwave imager data during tropical cyclones: comparisons of scattering index, regression, and support vector regression, J. Hydrometeorol., 13, 1567–1578, doi:10.1175/jhm-d-11-0118.1, 2012.
Wild, M.: Enlightening global dimming and brightening, B. Am. Meteorol. Soc., 93, 27–37, doi:10.1175/bams-d-11-00074.1, 2012.
Wu, G., Liu, Y., Zhang, Q., Duan, A., Wang, T., Wan, R., Liu, X., Li, W., Wang, Z., and Liang, X.: The influence of mechanical and thermal forcing by the Tibetan Plateau on Asian climate, J. Hydrometeorol., 8, 770–789, doi:10.1175/JHM609.1, 2007.
Wu, G., Liu, Y., He, B., Bao, Q., Duan, A., and Jin, F.: Thermal controls on the Asian summer monsoon, Sci. Rep., 2, 404, doi:10.1038/srep00404, 2012a.
Wu, H., Zhang, X., Liang, S., Yang, H., and Zhou, G.: Estimation of clear-sky land surface longwave radiation from MODIS data products by merging multiple models, J. Geophys. Res.-Atmos., 117, D22107, doi:10.1029/2012jd017567, 2012b.
Xue, B.-L., Wang, L., Li, X., Yang, K., Chen, D., and Sun, L.: Evaluation of evapotranspiration estimates for two river basins on the Tibetan Plateau by a water balance method, J. Hydrol., 492, 290–297, doi:10.1016/j.jhydrol.2013.04.005, 2013.

Yanai, M. and Li, C. F.: Mechanism of heating and the boundary layer over the Tibetan Plateau, Mon. Weather Rev., 122, 305–323, doi:10.1175/1520-0493(1994)122<0305:mohatb>2.0.co;2, 1994.

Yang, K. and Koike, T.: Satellite monitoring of the surface water and energy budget in the central Tibetan Plateau, Adv. Atmos. Sci, 25, 974–985, doi:10.1007/s00376-008-0974-8, 2008.

Yang, K., Koike, T., Fujii, H., Tamagawa, K., and Hirose, N.: Improvement of surface flux parametrizations with a turbulence-related length, Q. J. Roy. Meteor. Soc., 128, 2073–2087, doi:10.1256/003590002320603548, 2002.

Yang, K., Koike, T., and Yang, D. W.: Surface flux parameterization in the Tibetan Plateau, Bound.-Lay. Meteorol., 106, 245–262, doi:10.1023/a:1021152407334, 2003.

Yang, K., Koike, T., Ishikawa, H., and Ma, Y. M.: Analysis of the surface energy budget at a site of GAME/Tibet using a single-source model, J. Meteorol. Soc. Jpn., 82, 131–153, doi:10.2151/jmsj.82.131, 2004.

Yang, K., Koike, T., Ishikawa, H., Kim, J., Li, X., Liu, H., Liu, S., Ma, Y., and Wang, J.: Turbulent flux transfer over bare-soil surfaces: characteristics and parameterization, J. Appl. Meteorol. Clim., 47, 276–290, doi:10.1175/2007jamc1547.1, 2008.

Yang, K., Qin, J., Guo, X., Zhou, D., and Ma, Y.: Method development for estimating sensible heat flux over the Tibetan Plateau from CMA data, J. Appl. Meteorol. Clim., 48, 2474–2486, doi:10.1175/2009jamc2167.1, 2009.

Yang, K., Guo, X., He, J., Qin, J., and Koike, T.: On the climatology and trend of the atmospheric heat source over the Tibetan Plateau: an experiments-supported revisit, J. Climate, 24, 1525–1541, doi:10.1175/2010jcli3848.1, 2011a.

Yang, K., Guo, X., and Wu, B.: Recent trends in surface sensible heat flux on the Tibetan Plateau, Sci. China Ser. D., 54, 19–28, doi:10.1007/s11430-010-4036-6, 2011b.

Yang, K., Ye, B., Zhou, D., Wu, B., Foken, T., Qin, J., and Zhou, Z.: Response of hydrological cycle to recent climate changes in the Tibetan Plateau, Climatic Change, 109, 517–534, doi:10.1007/s10584-011-0099-4, 2011c.

Yang, W., Guo, X., Yao, T., Yang, K., Zhao, L., Li, S., and Zhu, M.: Summertime surface energy budget and ablation modeling in the ablation zone of a maritime Tibetan glacier, J. Geophys. Res., 116, D14116, doi:10.1029/2010jd015183, 2011d.

Yao, J., Zhao, L., Ding, Y., Gu, L., Jiao, K., Qiao, Y., and Wang, Y.: The surface energy budget and evapotranspiration in the Tanggula region on the Tibetan Plateau, Cold Reg. Sci. Technol., 52, 326–340, doi:10.1016/j.coldregions.2007.04.001, 2008.

Yao, J., Zhao, L., Gu, L., Qiao, Y., and Jiao, K.: The surface energy budget in the permafrost region of the Tibetan Plateau, Atmos. Res., 102, 394–407, doi:10.1016/j.atmosres.2011.09.001, 2011.

Yao, Y., Liang, S., Qin, Q., Wang, K., Liu, S., and Zhao, S.: Satellite detection of increases in global land surface evapotranspiration during 1984–2007, Int. J. Digit. Earth, 5, 299–318, doi:10.1080/17538947.2011.598953, 2012.

Ye, D. and Gao, Y.: The meteorology of the Qinghai–Xizang (Tibet) Plateau, Science Press, Beijing, 1979 (in Chinese).

Ye, D. and Wu, G.: The role of the heat source of the Tibetan Plateau in the general circulation, Meteorol. Atmos. Phys., 67, 181–198, doi:10.1007/bf01277509, 1998.

You, Q., Sanchez-Lorenzo, A., Wild, M., Folini, D., Fraedrich, K., Ren, G., and Kang, S.: Decadal variation of surface solar radiation in the Tibetan Plateau from observations, reanalysis and model simulations, Clim. Dynam., 40, 2073–2086, doi:10.1007/s00382-012-1383-3, 2013.

Yu, G. R., Wen, X. F., Sun, X. M., Tanner, B. D., Lee, X., and Chen, J. Y.: Overview of ChinaFLUX and evaluation of its eddy covariance measurement, Agr. Forest Meteorol., 137, 125–137, doi:10.1016/j.agrformet.2006.02.011, 2006.

Zhang, G., Kang, S., Fujita, K., Huintjes, E., Xu, J., Yamazaki, T., Haginoya, S., Wei, Y., Scherer, D., Schneider, C., and Yao, T.: Energy and mass balance of Zhadang glacier surface, central Tibetan Plateau, J. Glaciol., 59, 137–148, doi:10.3189/2013JoG12J152, 2013.

Zhang, K., Kimball, J. S., Mu, Q., Jones, L. A., Goetz, S. J., and Running, S. W.: Satellite based analysis of northern ET trends and associated changes in the regional water balance from 1983 to 2005, J. Hydrol., 379, 92–110, doi:10.1016/j.jhydrol.2009.09.047, 2009.

Zhang, K., Kimball, J. S., Nemani, R. R., and Running, S. W.: A continuous satellite-derived global record of land surface evapotranspiration from 1983 to 2006, Water Resour. Res., 46, W09522, doi:10.1029/2009wr008800, 2010.

Zhou, D. and Huang, R.: Response of water budget to recent climatic changes in the source region of the Yellow River, Chinese Sci. Bull., 57, 2155–2162, doi:10.1007/s11434-012-5041-2, 2012.

Zhu, X., Liu, Y., and Wu, G.: An assessment of summer sensible heat flux on the Tibetan Plateau from eight data sets, Sci. China Ser. D., 55, 779–786, doi:10.1007/s11430-012-4379-2, 2012.

Zou, H.: The adaptive lasso and its oracle properties, J. Am. Stat. Assoc., 101, 1418–1429, doi:10.1198/016214506000000735, 2006.

Zou, H., Ma, S., Zhou, L., Li, P., and Li, A.: Measured turbulent heat transfer on the northern slope of Mt. Everest and its relation to the south Asian summer monsoon, Geophys. Res. Lett., 36, L09810, doi:10.1029/2008gl036984, 2009.

ACPD
13, 30349–30405, 2013

Surface sensible and latent heat fluxes over the Tibetan Plateau

Q. Shi and S. Liang

Table 1. Summary of data sources (* for comparison).

Name	Organization/ institution	Spatial resolution/ stations	Temporal resolution	Temporal coverage
		Reanalysis datasets		
CFSR	NCEP	T382 (38 km)	hourly	Jan 1979–Dec 2009
MERRA	NASA	$0.50^{\circ} \times 0.67^{\circ}$	hourly	Jan 1979–Apr 2013
ERA-Interim	ECMWF	T255 (80 km)	3 hourly	Jan 1979–Mar 2013
JRA-25	JMA/CRIEPI	T106 (110 km)	3 hourly	Jan 1979–Dec 2011
MERRALAND*	NASA	$0.50^{\circ} \times 0.67^{\circ}$	hourly	Jan 1979–Apr 2013
NRA-1*	NCEP/NCAR	T62 (200 km)	6 hourly	Jan 1948–Jul 2012
NRA-2*	NCEP/NCAR	T62 (200 km)	6 hourly	Jan 1979–Dec 2011
GLADS-1_NOAH*	NCAR	1.00°	3 hourly	Jan 1979–May 2012
GLADS-2_NOAH*	NCAR	1.00°	3 hourly	Jan 1948–Dec 2008
GLADS-1_CLM*	NCAR	1.00°	3 hourly	Jan 1979–May 2012
GLADS-1_MOS*	NASA/GSFC	1.00°	3 hourly	Jan 1979–May 2012
		Remote sensing datasets		
Zhang10	NASA	8 km	monthly	Jan 1983–Dec 2006
PU-ET*	PU	0.50°	3 hourly	Jan 1984–Dec 2007
MTE-LE-H*	MPI	0.50°	monthly	Jan 1982–Dec 2011
		Ground-measured datasets		
AsiaFLUX	FLUXNET	1 stations	15 min	Jul 2002–Dec 2004
ChinaFLUX	FLUXNET	3 station	30 min	Nov 2002–Dec 2007
GAME-Tibet	AAN	10 stations	30 min	Dec 1994–Apr 2005
CAMP-Tibet	CEOP	9 stations	10 min, hourly	Oct 2002–Dec 2004
Yang09, Yang11*	ITPR CAS	85 stations	daily	Jan 1984–Dec 2006

Discussion Paper | Discussion Paper | Discussion Paper | Discussion Paper |
ACPD
13, 30349–30405, 2013
Surface sensible and latent heat fluxes over the Tibetan Plateau
Q. Shi and S. Liang
Title Page
Abstract Introduction
Conclusions References
Tables Figures
◀◀ ▶▶
◀ ▶
Back Close
Full Screen / Esc
Printer-friendly Version
Interactive Discussion

Table 2. Information of the ground observation sites over the TP with measurement of latent heat flux (LE), sensible heat flux (*H*), and ground heat flux (*G*).

Name	Lat (° N)	Lon (° S)	Ele (m)	Measured variable	Height	Instruments	Data period	Date length
						AsiaFlux		
HBM	37.61	101.31	3250	LE, *H*	2.2 m	Campbell CSAT-3, LI-COR LI-7500	Jul 2002–Dec 2004	519
				G	−0.01 m	Campbell HFT-3		942
						CAMP/Tibet		
Amdo	32.24	91.62	4695	*G*	−0.10 m	EKO MF-81	Oct 2002–Dec 2004	520
ANNI	31.25	92.17	4480	*G*	−0.10 m	EKO MF-81	Oct 2002–Dec 2004	328
D105	33.06	91.94	5038	*G*	−0.10 m	EKO MF-81	Oct 2002–Dec 2004	765
MS3478	31.92	91.71	4619	*G*	−0.10 m	EKO MF-81	Oct 2002–Dec 2004	820
BJ	31.37	91.90	4509	LE, *H*	3.00 m	Kaijo DA-600, LI-COR LI-7500	Oct 2002–Dec 2004	51
				G	−0.10 m	EKO MF-81		654
Gaize	32.30	84.05	4416	*G*	−0.03 m	EKO MS-802, EKO MS-202	Oct 2002–Dec 2004	582
						EKO MF-81		698
						ChinaFLUX		
DX	30.50	91.07	4751	LE, *H*	2.2 m	Campbell CSAT-3, LI-COR LI-7500	Jun 2003–Dec 2007	1097
				G	−0.05 m	Hukseflux HFP01		597
HBS	37.67	101.33	3400	LE, *H*	2.2 m	Campbell CSAT-3, LI-COR LI-7500	Dec 2002–Dec 2007	1107
				G	−0.05 m	Hukseflux HFP01		1726
						GAME/Tibet		
Amdo	32.24	91.63	4700	LE, *H*	2.85 m	Kaijo DA-300, Kaijo AH-300	Jan 1998–May 2003	47
				G	−0.10 m	EKO MF-81		1612
MS3478	31.93	91.72	5063	LE, *H*	2.85 m	GILL SAT-R3A, Vaisala 50Y Bandpass TRH	May 1998–Sep 1998	40
				G	−0.01 m	Campbell HFT-3		118
Gaize	32.30	84.05	4420	*G*	−0.25 m	EKO MF-81	May 1998–Sep 1998	117
BJ	31.37	91.90	4580	LE, *H*	2.85 m	Campbell CSAT-3, Campbell KH20	May 1998–Sep 1998	30
				G	−0.05 m	Campbell HFT-3		89

ACPD
13, 30349–30405, 2013

Surface sensible and latent heat fluxes over the Tibetan Plateau

Q. Shi and S. Liang

Table 3. Validation results of the surface energy budget components of reanalysis and remote sensing datasets.

		CFSR	MERRA	ERA-Interim	JRA-25	Zhang10
Sensible heat flux	RMSE ($W m^{-2}$)	22.0	28.7	20.5	29.9	–
	MBE ($W m^{-2}$)	−4.9	4.4	−11.8	−14.5	–
	R^2	0.32	0.12	0.28	0.23	–
Latent heat flux	RMSE ($W m^{-2}$)	23.8	15.4	11.5	15.0	22.1
	MBE ($W m^{-2}$)	−13.1	8.5	−1.7	3.9	−12.0
	R^2	0.82	0.87	0.90	0.86	0.89
Ground heat flux	RMSE ($W m^{-2}$)	11.9	6.3	10.4	8.5	–
	MBE ($W m^{-2}$)	6.6	−1.8	0.1	−0.5	–
	R^2	0.73	0.78	0.73	0.82	–

ACPD
13, 30349–30405, 2013

Table 4. Coefficients and intercept to calculate fused data (coefficients and intercepts with p value < 0.05 are in bold).

	Intercept ($W m^{-2}$)	CFSR	MERRA	ERA-Interim	JRA-25	Zhang10
Latent heat flux	**−8.7994**	–	**0.4191**	**0.5345**	0.1961	–
	−10.3056	–	**0.3197**	**0.3112**	**0.2398**	**0.4962**
Ground heat flux	**1.4429**	**−0.0732**	**0.1422**	–	**0.3531**	–

ACPD
13, 30349–30405, 2013

Surface sensible and latent heat fluxes over the Tibetan Plateau

Q. Shi and S. Liang

Table 5. Comparison of the cross validation results of the surface energy budget from the fused data, reanalysis, and remote sensing datasets.

Products	Sensible heat flux ($W m^{-2}$)	Latent heat flux ($W m^{-2}$)	Ground heat flux ($W m^{-2}$)
Fusion, MLR	17.8	11.1	2.6
Fusion, MLR close Bowen ratio	23.0	20.6	2.6
Fusion, stepwise	18.1	11.3	2.6
Fusion, Lasso	17.2	10.9	2.6
Fusion, PCA_2	20.5	8.8	2.6
Fusion, PCA_3	17.6	9.7	2.6
Fusion, BMA	17.0	10.5	2.6
Fusion, RF	17.6	9.1	2.8
Fusion, SVM	16.9	9.3	2.7
CFSR	22.9	17.0	11.9
MERRA	25.6	14.1	6.3
ERA-Interim	30.4	11.5	10.4
JRA-25	24.8	14.7	8.5
Zhang10	18.7	14.7	5.6
MERRALAND	32.3	14.1	6.3
GLADS-1_CLM	27.5	16.9	8.6
GLADS-1_MOS	22.4	13.8	9.4
GLADS-1_NOAH	34.7	30.4	5.3
GLADS-2_NOAH	21.8	17.0	13.5
NRA-1	74.1	59.0	21.0
NRA-2	74.0	48.2	18.9
PU-LE	15.2	20.1	–
MTE-LE-H	35.8	31.7	–

ACPD
13, 30349–30405, 2013
Surface sensible and latent heat fluxes over the Tibetan Plateau
Q. Shi and S. Liang

Title Page
Abstract | Introduction
Conclusions | References
Tables | Figures
◀◀ | ▶▶
◀ | ▶
Back | Close
Full Screen / Esc
Printer-friendly Version
Interactive Discussion

Table 6. Decadal changes of latent and sensible heat fluxes over the TP (p value < 0.05 are in bold).

	Annual	Spring	Summer	Autumn	Winter
Sensible heat flux ($W m^{-2} decade^{-1}$)					
Yang11	**−1.5**	**−2.4**	**−2.6**	−0.6	**−0.7**
CFSR	−2.5	−4.3	**−4.0**	−1.8	0.6
MERRA	0.6	−0.4	0.0	**2.0**	0.3
ERA-Interim	**−1.4**	**−1.6**	**−1.9**	**−1.2**	−1.2
JRA-25	**−2.1**	**−3.1**	−2.1	−1.1	**−3.4**
Zhang10	**−9.3**	**−4.8**	**−12.5**	**−9.9**	**−7.0**
This study (CMA stations)	**−1.9**	0.1	**−4.5**	**−3.3**	0.8
This study (regional)	**−1.1**	1.0	**−3.9**	**−1.8**	0.2
Latent heat flux ($W m^{-2} decade^{-1}$)					
Yang11	**1.0**	**1.7**	0.3	1.3	**1.3**
CFSR	**1.8**	2.7	**2.0**	**2.0**	0.6
MERRA	−0.1	−0.3	1.0	−0.3	−0.5
ERA-Interim	0.2	−0.8	−0.6	**2.0**	0.1
JRA-25	**2.5**	**2.8**	**3.7**	**2.9**	**1.6**
Zhang 10	**−1.5**	**−2.3**	**−3.9**	−0.2	0.2
This study (CMA stations)	−0.1	−0.8	−0.9	1.1	0.4
This study (regional)	0.1	**−0.7**	0.0	**1.0**	0.0

ACPD
13, 30349–30405, 2013

Table 7. Correlation coefficients between sensible and latent heat fluxes and surface and atmospheric anomalies (net shortwave (SW) and longwave (LW), all-wave radiation are from Shi and Liang, 2013a) over the TP (p value < 0.05 are in bold).

	Annual	Spring	Summer	Autumn	Winter
Sensible heat flux, cloud cover	**−0.45**	−0.30	**−0.39**	**−0.38**	**−0.42**
Sensible heat flux, water vapor	**−0.39**	**0.50**	**−0.52**	**−0.40**	**−0.46**
Sensible heat flux, GIMMS NDVI	−0.18	−0.29	**−0.39**	0.28	**0.41**
Sensible heat flux, temperature range	0.31	0.20	**0.58**	**0.61**	0.15
Sensible heat flux, mean temperature	−0.32	**0.45**	**−0.42**	**−0.52**	−0.31
Sensible heat flux, snow cover	−0.23	0.27	−0.08	−0.20	−0.33
Sensible heat flux, net SW radiation	**0.65**	**0.79**	**0.70**	**0.53**	**0.50**
Sensible heat flux, net LW radiation	−0.13	−0.07	**−0.46**	−0.19	−0.14
Sensible heat flux, net radiation	**0.72**	**0.91**	**0.73**	**0.64**	**0.88**
Latent heat flux, cloud cover	**0.52**	**0.41**	0.17	**0.37**	**0.39**
Latent heat flux, water vapor	**0.48**	−0.09	0.19	**0.85**	**0.65**
Latent heat flux, GIMMS NDVI	**0.59**	**0.53**	**0.73**	**0.42**	0.32
Latent heat flux, temperature range	**−0.42**	−0.17	−0.02	−0.28	−0.22
Latent heat flux, mean temperature	0.18	−0.35	0.16	**0.70**	**0.48**
Latent heat flux, maximum temperature	0.06	−0.34	0.15	**0.76**	0.36
Latent heat flux, snow cover	0.34	0.13	0.18	0.00	0.16
Latent heat flux, net SW radiation	−0.04	−0.01	0.11	−0.05	0.05
Latent heat flux, net LW radiation	**0.45**	0.33	0.11	0.31	−0.06
Latent heat flux, net radiation	**0.41**	0.22	0.33	0.34	−0.01

ACPD
13, 30349–30405, 2013

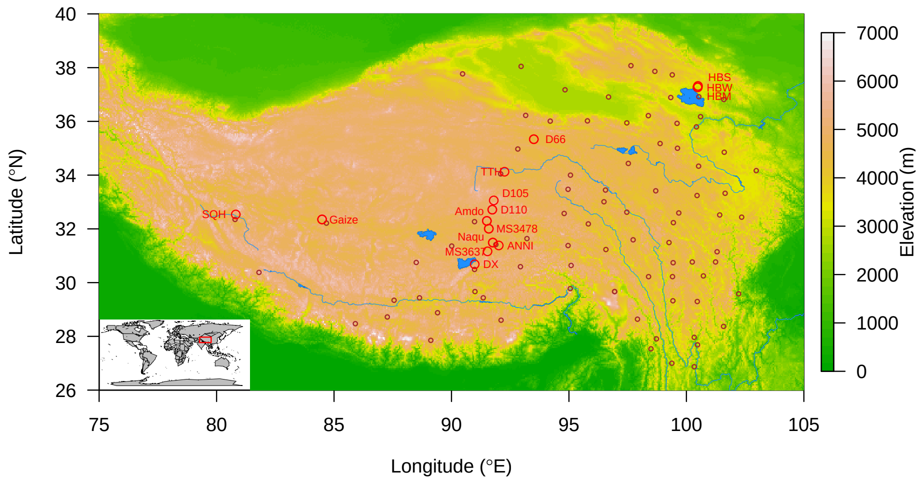

Fig. 1. Study area with major lakes, rivers, six regions, validation sites (red circle), and CMA sites for comparison (black circle).

ACPD
13, 30349–30405, 2013

Surface sensible and latent heat fluxes over the Tibetan Plateau

Q. Shi and S. Liang

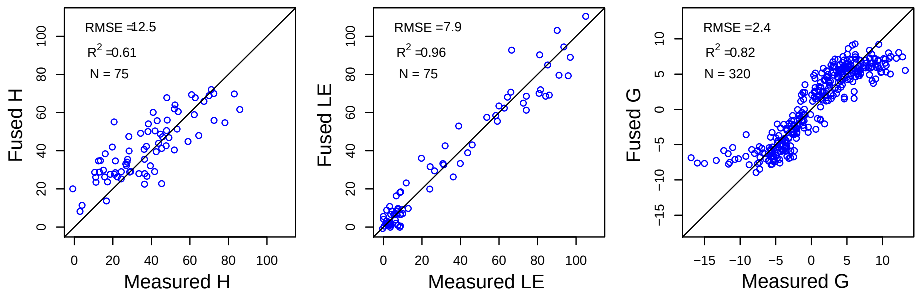

Fig. 2. Scatterplot of sensible heat flux (*H*), latent heat flux (LE), and ground heat flux (*G*) of fused data with ground measurement.

ACPD
13, 30349–30405, 2013

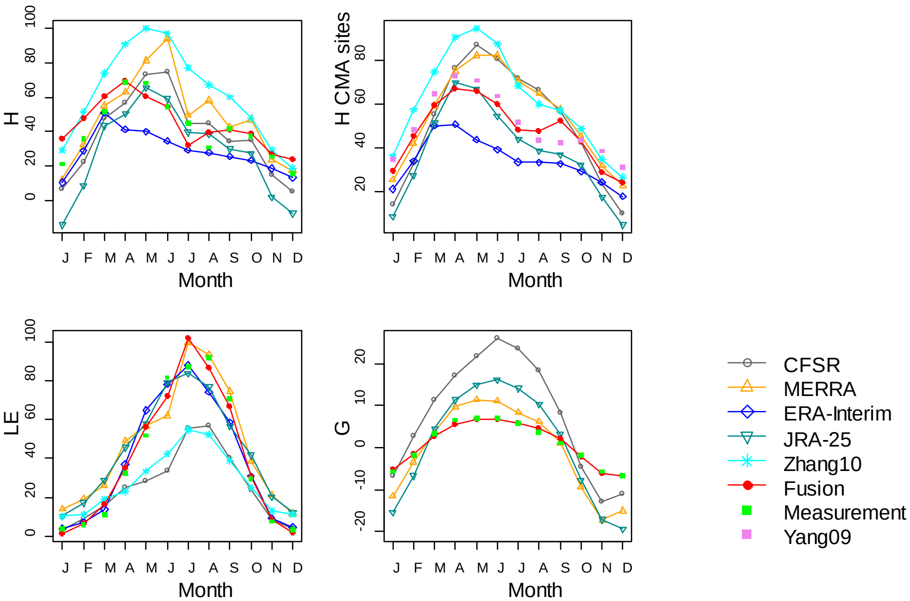

Fig. 3. Monthly cycles of sensible heat flux (H), latent heat flux (LE), and ground heat flux (G) from multiple datasets and fused data with ground measurement averaged for all available sites.

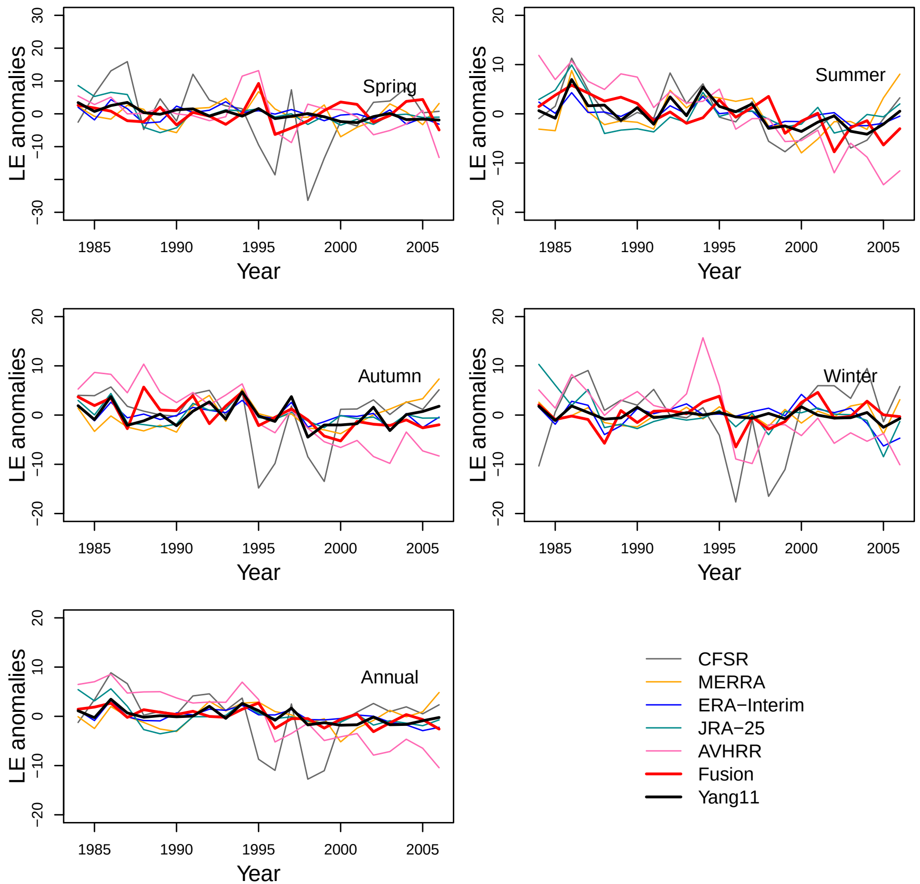

Fig. 4. Anomalies of sensible heat flux from multiple datasets and fused data with ground measurement averaged for all available CMA stations.

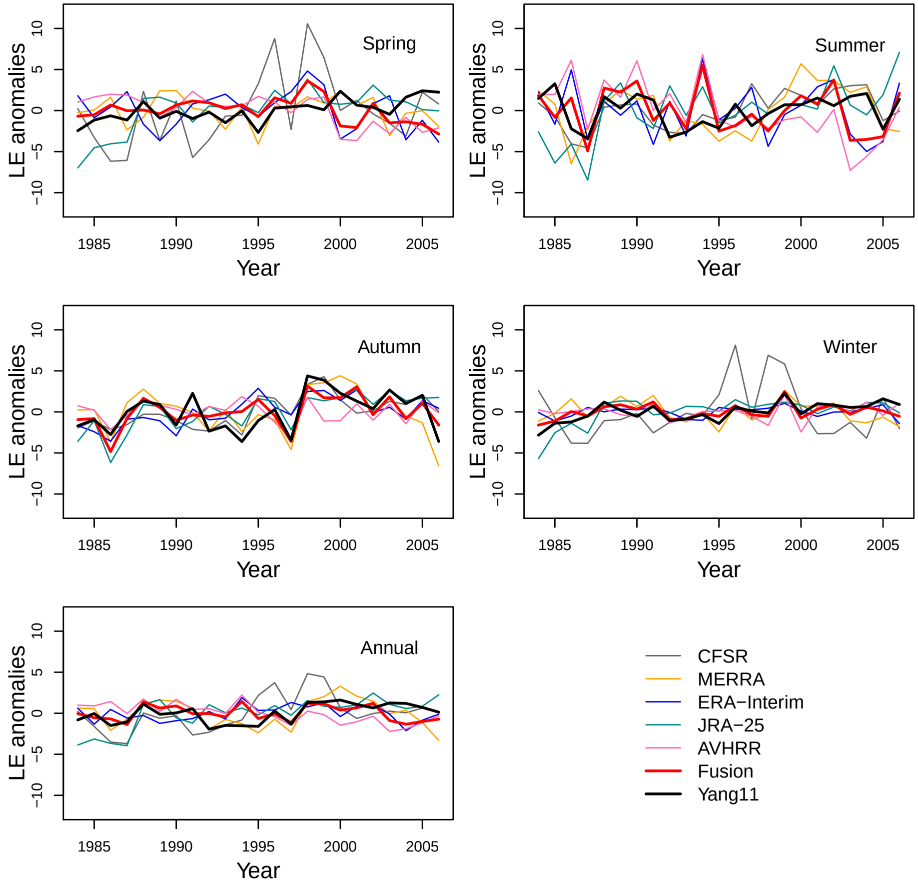

Fig. 5. Anomalies of latent heat flux from multiple datasets and fused data with ground measurement averaged for all available CMA stations.

ACPD
13, 30349–30405, 2013

Surface sensible and latent heat fluxes over the Tibetan Plateau

Q. Shi and S. Liang

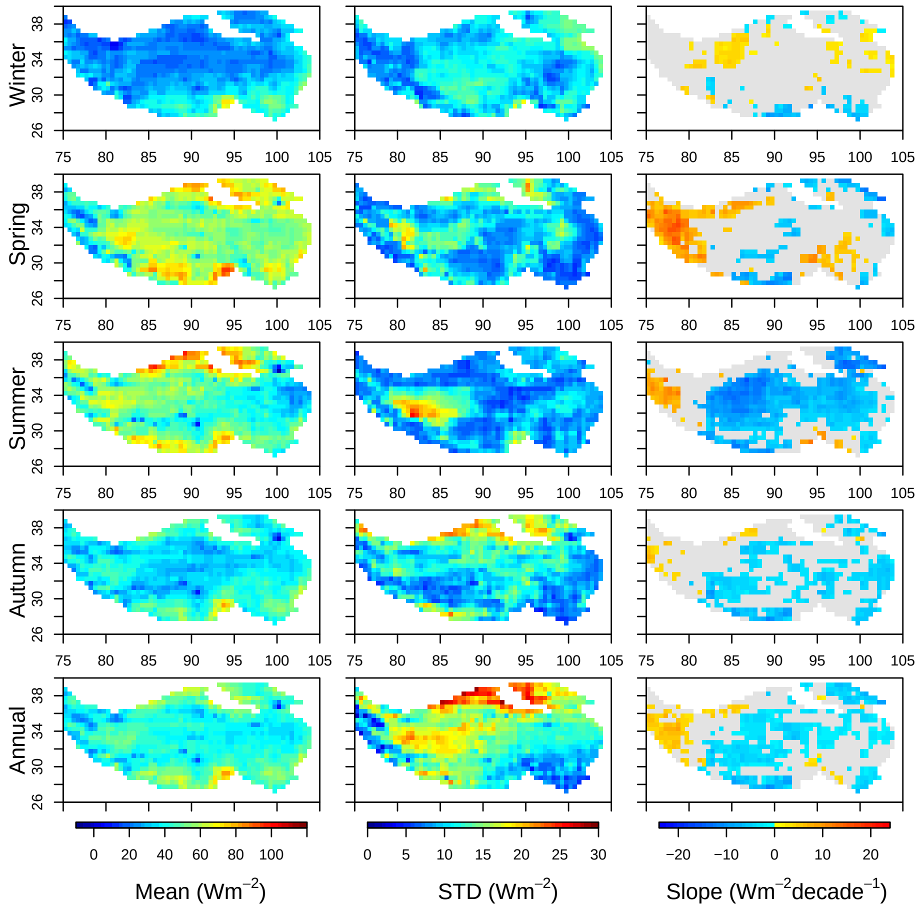

Fig. 6. Spatial distribution of seasonal/annual mean, STD, and decadal changes for sensible heat flux over the Tibetan Plateau.

ACPD
13, 30349–30405, 2013

Surface sensible and latent heat fluxes over the Tibetan Plateau

Q. Shi and S. Liang

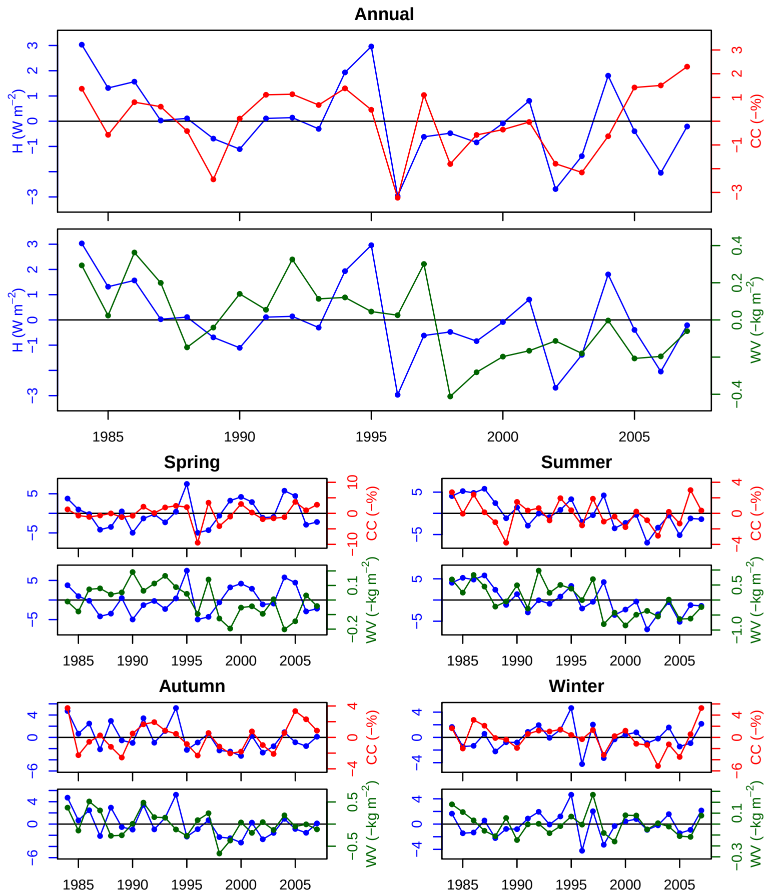

Fig. 7. Temporal variation of seasonal and annual sensible heat flux (*H*), cloud cover (CC), and water vapor (WV) anomalies over the TP.

ACPD
13, 30349–30405, 2013

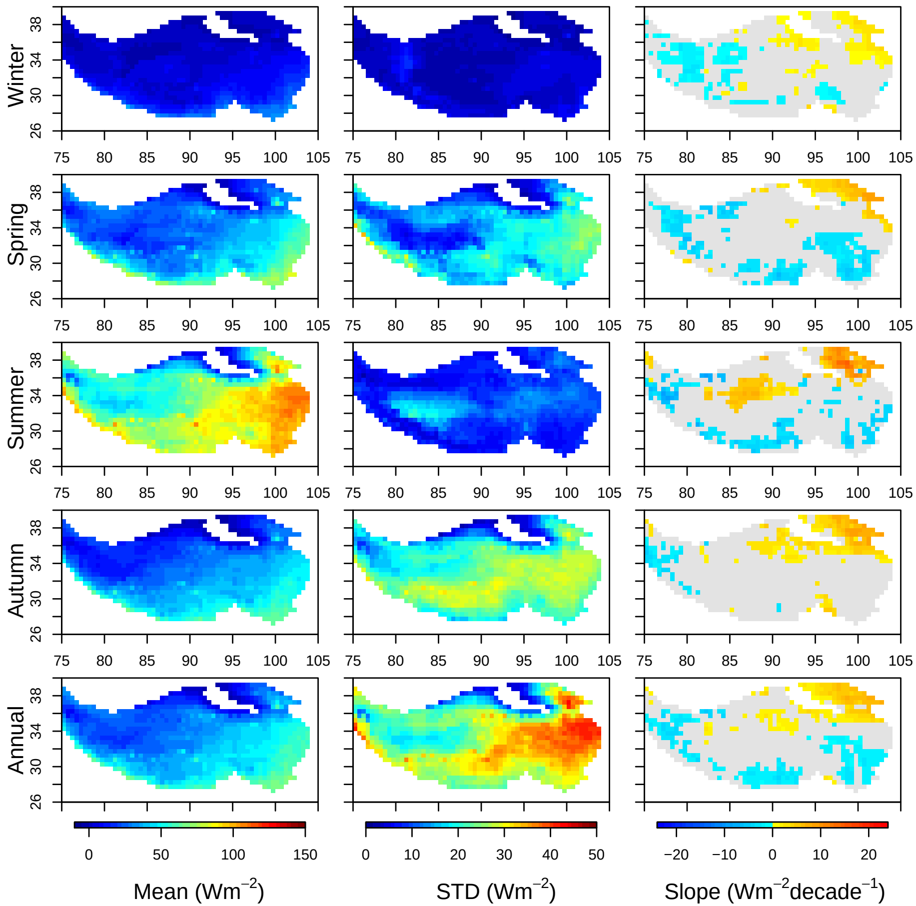

Fig. 8. Spatial distribution of mean, STD, and decadal changes of latent heat flux over the TP (1984–2007).

ACPD
13, 30349–30405, 2013

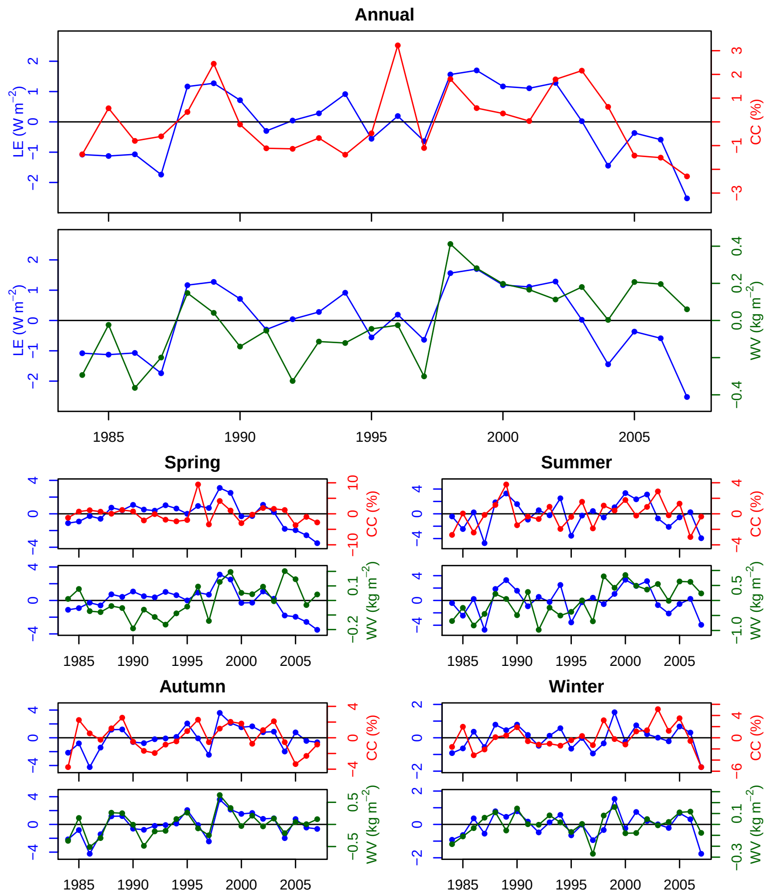

Fig. 9. Temporal variation of seasonal and annual latent heat flux (LE), cloud cover (CC), and water vapor (WV) anomalies over the TP.

ACPD
13, 30349–30405, 2013

Surface sensible and latent heat fluxes over the Tibetan Plateau

Q. Shi and S. Liang

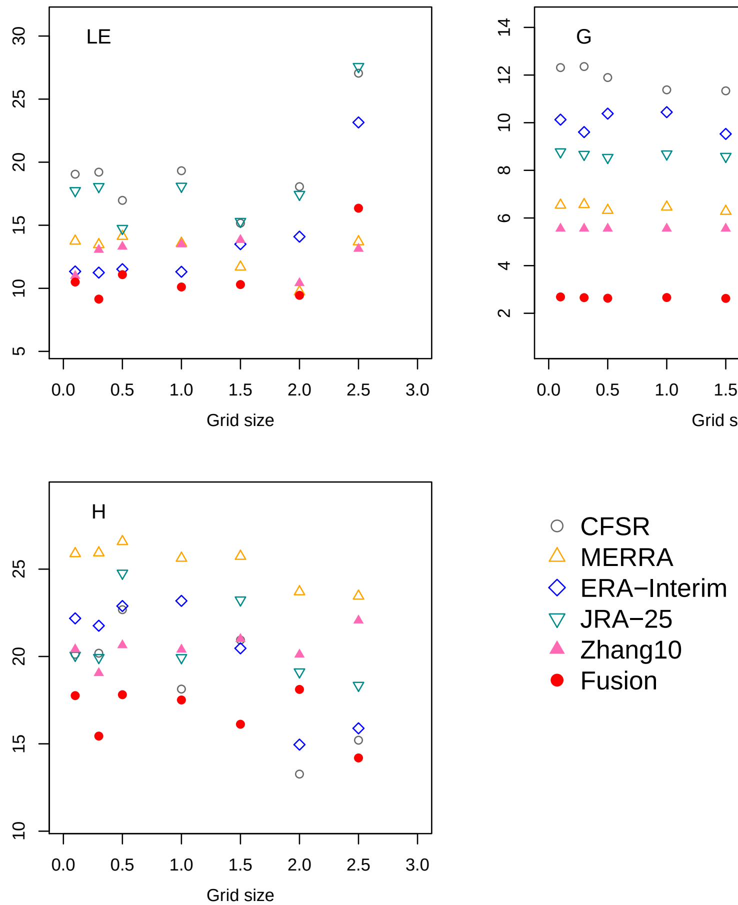

Fig. 10. Comparison of the RMSE_CV ($W\,m^{-2}$) of latent heat flux (LE), ground heat flux (G), and sensible heat flux (H) at multiple grid sizes (°) from original datasets and fused data.

ACPD
13, 30349–30405, 2013